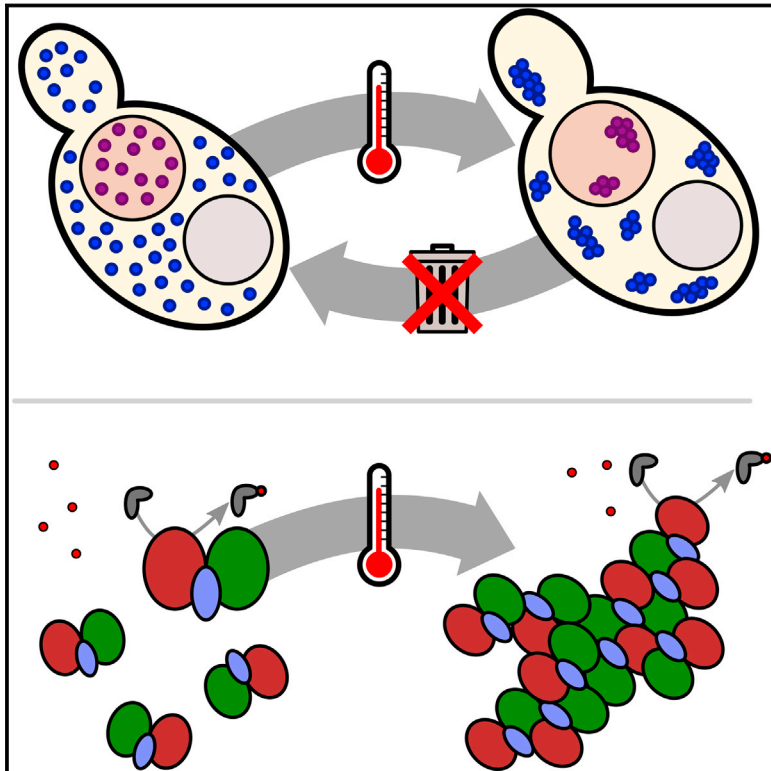


Reversible, Specific, Active Aggregates of Endogenous Proteins Assemble upon Heat Stress

Graphical Abstract



Authors

Edward W.J. Wallace,
 Jamie L. Kear-Scott,
 Evgeny V. Pilipenko, ..., Tao Pan,
 Bogdan A. Budnik, D. Allan Drummond

Correspondence

dadrummond@uchicago.edu

In Brief

The aggregates of endogenous proteins triggered by heat stress in yeast are reversible. Rather than representing irreparably misfolded proteins destined for degradation, they can maintain activity and re-solubilize, suggesting an adaptive strategy underlying aggregation.

Highlights

- Mass spectrometry quantifies aggregation of endogenous proteins during heat stress
- Aggregates form rapidly in specific subcellular compartments
- Endogenous protein aggregates are disassembled without degradation during recovery
- In vitro, a heat-aggregated enzyme complex retains activity and fidelity



Reversible, Specific, Active Aggregates of Endogenous Proteins Assemble upon Heat Stress

Edward W.J. Wallace,¹ Jamie L. Kear-Scott,¹ Evgeny V. Pilipenko,¹ Michael H. Schwartz,¹ Pawel R. Laskowski,¹ Alexandra E. Rojek,^{1,2} Christopher D. Katanski,¹ Joshua A. Riback,¹ Michael F. Dion,³ Alexander M. Franks,⁴ Edoardo M. Airoidi,^{3,4} Tao Pan,¹ Bogdan A. Budnik,³ and D. Allan Drummond^{1,*}

¹Department of Biochemistry and Molecular Biology, The University of Chicago, 929 East 57th Street, Chicago, IL 60637, USA

²Department of Molecular and Cellular Biology, Harvard University, Cambridge, MA 02138, USA

³FAS Center for Systems Biology, Harvard University, Cambridge, MA 02138, USA

⁴Department of Statistics, Harvard University, Cambridge, MA 02138, USA

*Correspondence: dadrummond@uchicago.edu

<http://dx.doi.org/10.1016/j.cell.2015.08.041>

SUMMARY

Heat causes protein misfolding and aggregation and, in eukaryotic cells, triggers aggregation of proteins and RNA into stress granules. We have carried out extensive proteomic studies to quantify heat-triggered aggregation and subsequent disaggregation in budding yeast, identifying >170 endogenous proteins aggregating within minutes of heat shock in multiple subcellular compartments. We demonstrate that these aggregated proteins are not misfolded and destined for degradation. Stable-isotope labeling reveals that even severely aggregated endogenous proteins are disaggregated without degradation during recovery from shock, contrasting with the rapid degradation observed for many exogenous thermolabile proteins. Although aggregation likely inactivates many cellular proteins, in the case of a heterotrimeric aminoacyl-tRNA synthetase complex, the aggregated proteins remain active with unaltered fidelity. We propose that most heat-induced aggregation of mature proteins reflects the operation of an adaptive, autoregulatory process of functionally significant aggregate assembly and disassembly that aids cellular adaptation to thermal stress.

INTRODUCTION

Following heat shock—a rapid increase in temperature to stressful but non-lethal levels—cells accumulate protein aggregates, decelerate protein synthesis, and mount a transcriptional program called the heat-shock response. Upregulated transcripts encode so-called heat-shock proteins, of which many are molecular chaperones. The standard interpretation of these events is that heat causes endogenous (species-native) proteins to misfold into aggregation-prone species whose toxicity is mitigated

and reversed by chaperones (Lindquist, 1986; Mogk et al., 1999; Vabulas et al., 2010; Verghese et al., 2012). Misfolding here refers to the deleterious loss of—or failure to attain—natively folded protein structure, sometimes by adopting stable non-native conformations.

Newly synthesized proteins are particularly susceptible to heat-induced misfolding and aggregation and appear to be the major triggers of the heat-shock response, as well as the main beneficiaries of its induction (Baler et al., 1992; Vabulas et al., 2010). In agreement, heat triggers rapid degradation of newly synthesized proteins, but not of bulk cellular protein (Medicherla and Goldberg, 2008).

Mature, folded proteins also aggregate in response to heat shock, forming protein/poly(A)⁺-RNA structures called heat-shock granules (HSGs). Discovered in plants (Nover et al., 1983), HSGs form upon robust heat shock in a range of eukaryotes, including budding yeast, trypanosome, insect, and mammalian cells (Grousl et al., 2009, 2013; Cherkasov et al., 2013; Farny et al., 2009). HSGs are functionally defined by their components, notably poly(A)-binding protein and eukaryotic initiation factor 4G; some components are common to RNA/protein granules formed during other stresses (Buchan et al., 2010, 2011; Kedersha and Anderson, 2002). The mechanism(s) of HSG formation remain unclear.

Many studies demonstrate aggregation and degradation of exogenous (heterologous or other non-species-native) proteins (Cherkasov et al., 2013; Heck et al., 2010; Fredrickson et al., 2013). Colocalization of exogenous aggregated proteins and HSGs has been interpreted as signaling the presence of endogenous misfolded proteins in HSGs (Cherkasov et al., 2013). However, the identities and folding states of HSG-associated proteins are largely unknown.

When cells return to lower temperatures, HSG dissolution is promoted by the disaggregase Hsp104 and the chaperone Hsp70 (Cherkasov et al., 2013), which also disaggregate misfolded proteins *in vitro* (Glover and Lindquist, 1998). It is unknown what fraction of disaggregated proteins are degraded *in vivo*, although evidence that stress granules are degraded by autophagy (Buchan et al., 2013) suggests that degradation might be the dominant fate of stress-induced aggregates.

Here, using the model eukaryote budding yeast (*Saccharomyces cerevisiae*), we report the results of experiments aimed at answering many of these fundamental questions. Which endogenous proteins aggregate during heat shock, and how do proteins differ in their propensity to aggregate? What is the relationship between protein aggregation and the formation of granules and other large subcellular foci? How does heat affect the function and fidelity of proteins determined to aggregate in response to heat shock *in vivo*? And what are the fates of endogenous aggregated proteins after heat shock?

RESULTS

Aggregation Profiling Identifies Many Thermally Sensitive Proteins

We quantified aggregation of proteins into high-molecular-weight particles by biochemical separation into supernatant and pellet fractions using ultracentrifugation, stable-isotope labeling, and liquid chromatography coupled to tandem mass spectrometry (LC-MS/MS) (Figure 1A). With these data, we estimated the proportion of each protein in the supernatant (pSup) using a statistical method that controls for differences in fraction mixing and inter-experiment variability (Experimental Procedures and Figure S1). Here and throughout, we refer to pelletable species of proteins that are soluble before heat shock as “aggregates,” without prejudging whether the particles result from misfolding, formation of protein/RNA granules, or other homogeneous or heterogeneous oligomerization processes.

We quantified protein aggregation in cells transferred from 30°C to 46°C for 2, 4, and 8 min and to 37°C and 42°C for 8 min (Figure 1 and Table S1). During these treatments, which are shorter than those typically used to study HSG formation (Grousl et al., 2009; Cherkasov et al., 2013; Supplemental Experimental Procedures), genes upregulated in the transcriptional heat-shock response show no significant change in protein levels (Figure S2A). By contrast, aggregation is rapid and widespread and increases with time and temperature (Figures 1B and 1C).

Heat Triggers Rapid and Specific Protein Aggregation

In the 46°C time course, 982 proteins are detected with at least two unique peptides at all time points (“well-detected,” 73% of the proteome by mass, 17% of verified open reading frames [Cherry et al., 2012]), upon which we focus. Most cellular proteins remain in the supernatant throughout (Figure 1B), and cytosolic and ribosomal proteins are the most enriched gene ontology (GO) terms describing these proteins (Figure S3). Proteins found in the pellet in all conditions are primarily membrane associated (Figure S3). Heat triggers the aggregation of a large group of proteins (177 well-detected proteins), classified by consistent and substantial movement from the supernatant in unheated cells to the pellet after a shift to 46°C (Table S3 and Experimental Procedures). Only four proteins moved from pellet to supernatant in the same interval (Table S4).

Of 18 HSG components identified in the literature (Table S2), we detected all but one (Ngr1). Twelve of these meet our criteria

for heat-triggered aggregation, including poly(A)-binding protein (Pab1), eIF4G/Tif4631, and eIF3, where our data show aggregation of all five stably complexed eIF3 subunits (Nip1/Rpg1/Prt1, reported previously [Grousl et al., 2009], and Tif34/Tif35 reported here) and eukaryotic release factors eRF1/Sup45 and eRF3/Sup35 (Figure S4A). Of the remaining five, Whi3 is not well detected but aggregates, and three proteins (Dhh1, eIF4G2/Tif4632, and small-subunit ribosomal protein Rps30A/B) do not clearly aggregate. The behavior of Rps30A/B is consistent with the lack of aggregation in 82 other well-detected ribosomal gene products from both subunits and with *in situ* hybridization against ribosomal RNA (Cherkasov et al., 2013). Our experimental conditions therefore allow us to quantify biochemically the aggregation of proteins reported to form HSGs by fluorescence microscopy.

In our data, 17 proteins aggregate more than any previously reported HSG component after 2 min heat shock at 46°C; we dub these “superaggregators” (Table S3 and Experimental Procedures). For example, the nuclear protein Ett1 plunges from a supernatant proportion of 0.93 to 0.15 after 2 min at 46°C, while the mRNA-binding protein Gbp2 drops from 0.8 to 0.25. In the same interval, HSG-forming proteins such as Pab1 and eIF3 remain mostly soluble (Figures 1C and S4). Notably, most superaggregators also show clear aggregation after 8 min at 37°C and 42°C (Figures 1C and 1D). At these temperatures and times, Pab1-marked HSGs do not form (Cherkasov et al., 2013).

GO terms enriched in heat-aggregating proteins include the molecular functions RNA binding (exemplified by poly(A)-binding protein Pab1 along with Npl3, Pub1, and Gbp2) and RNA helicase activity (seven proteins, including Ded1 and Dbp2/3) (Figure S3). Enriched cellular components include cytosolic stress granules, polysomes, and notably the nucleolus (16 nucleolar proteins).

Six aminoacyl-tRNA-synthetases aggregate, including the yeast multisynthetase complex composed of methionyl- and glutamyl-tRNA synthetases Mes1 and Gus1 bound together by the aminoacylation cofactor Arc1. We return to this complex later.

Molecular chaperones, which colocalize with HSGs, largely remain soluble in our data, suggesting a biochemical distinction between aggregation and recruitment to aggregates. However, notable exceptions exist, including the ribosome-associated chaperone complex (RAC) discussed later. The small heat-shock proteins Hsp26 and Hsp42, despite poor detection in our dataset, partition into the pellet upon heat shock (Figure S4A).

Endogenous Proteins Aggregate in Distinct Compartments

To determine the subcellular location and morphology of aggregates for MS-identified aggregators, we imaged yeast strains engineered with fluorescent C-terminally tagged proteins at their native chromosomal loci. We tagged select proteins with mRuby2, a red fluorescent protein, and tagged the HSG marker Pab1 with Clover, a green fluorescent protein (Lam et al., 2012), mating these strains to form dual-tagged diploids (Figure 2A). Fusions of the non-aggregating glycolytic enzyme Pkg1 stay cytosolic and diffuse when heat shocked, and diploids bearing

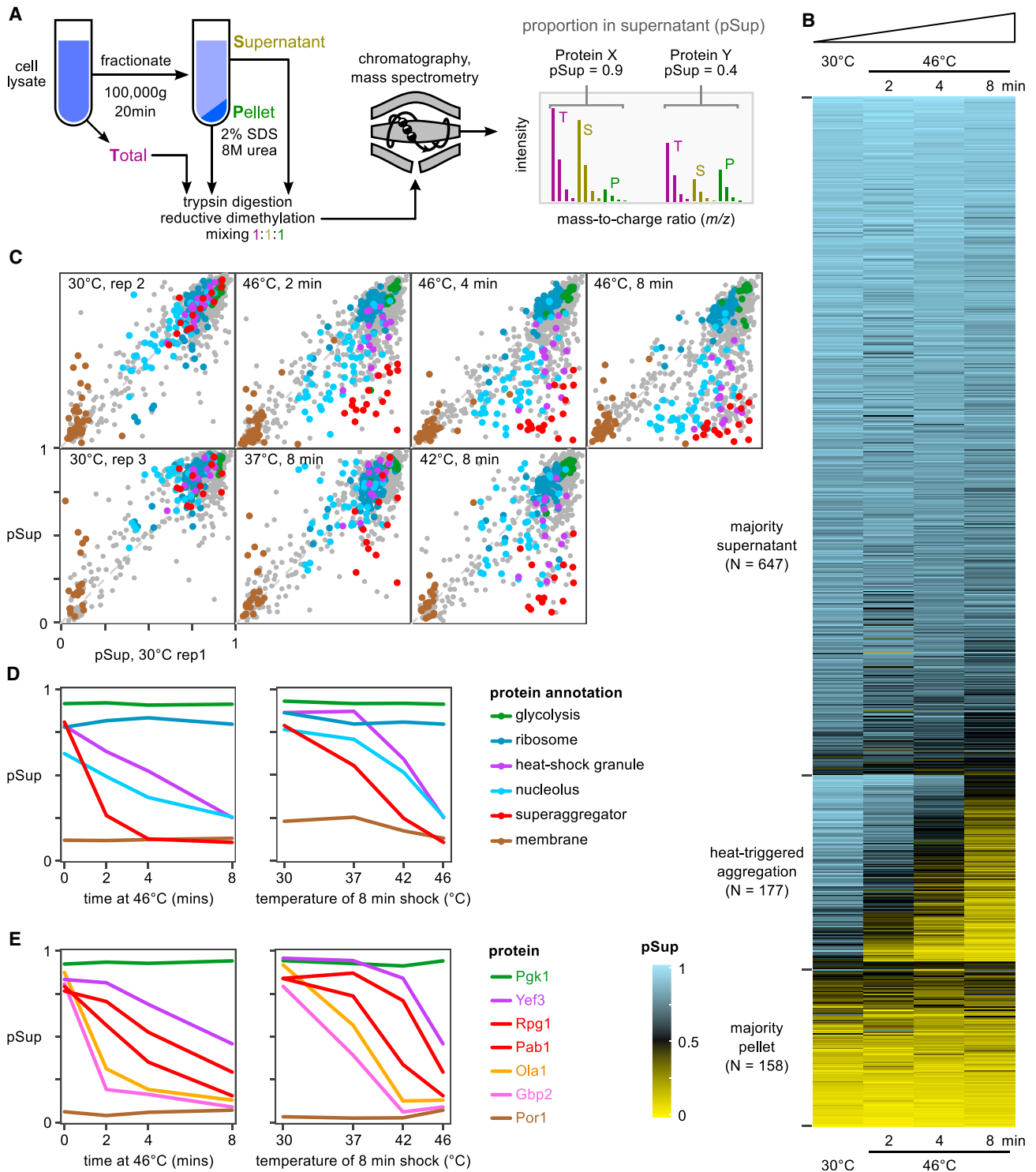


Figure 1. Proteome-wide Aggregation Profiling

(A) Aggregation profiling by isotope labeling and mass spectrometry yields estimates of the proportion of each protein in the supernatant (pSup) before and after thermal stress.

(B) pSup values in the 46°C time course for all well-detected proteins show proteins consistently found in the supernatant (top), consistently found in the pellet (bottom), and transitioning from supernatant to pellet during the 8 min heat shock (middle, see text).

(legend continued on next page)

Pab1 tagged with both fluorophores (no untagged Pab1 present) form cytosolic foci containing both colored tags (Figure 2B), indicating that these fluorophores neither cause nor prevent aggregation.

Proteins detected to aggregate by mass spectrometry after an 8 min 46°C heat shock also form foci (Figures 2B and 2C). Mes1 and Gus1, components of the multisynthetase complex, form cytosolic foci colocalized with Pab1. Arc1, the third multisynthetase component, likewise forms fluorescent foci colocalized with Gus1 (Figure 2C). Ola1, a superaggregating cytosolic protein previously implicated in translation termination (Samanfar et al., 2014), also forms foci colocalized with Pab1. These four proteins are all thus bona fide heat-shock granule components.

Some heat-aggregating proteins form nuclear foci. Gbp2, a nuclear poly(A)-RNA-binding protein involved in nuclear-cytoplasmic mRNA transport, forms sub-nuclear granules during heat shock (Figure 2B). Fpr3, a nucleolar component adopting the diagnostic nucleolar crescent shape under non-shock conditions, becomes increasingly granular within the nucleolus during heat shock (Figure 2B). Ett1, a nuclear protein and the most rapidly aggregating protein detected by mass spectrometry, forms nuclear foci during heat shock (Figure 2B) which colocalized with Gar1, a nucleolar protein that shows no heat-triggered aggregation by MS (Figure S5A). These results suggest that Ett1 aggregates in or near the nucleolus upon heat shock, possibly consistent with localization to the intranuclear quality-control compartment (INQ) (Miller et al., 2015a). We often observe multiple Ett1 foci per cell (Figure S5C).

Translation Inhibition Impedes Granule Formation but Does Not Prevent Stress-Triggered Protein Aggregation

Our data indicate clear distinctions between the heat-triggered *in vivo* formation of fluorescent foci and of submicroscopic, biochemically detectable aggregates. After milder shocks, several proteins producing pelletable aggregates did not form foci, such as Ett1 (at 37°C) and Pab1 (at 42°C) (Figures S5B and S5C). Also, Hsp104 forms foci co-localized with Pab1 upon heat shock (Cherkasov et al., 2013) while remaining highly soluble (Figure S4A), showing its recruitment to, but not stable association with, substrates within heat-shock granules.

A series of studies has demonstrated the preferential retention of cytosolic heat-induced protein aggregates by mother cells during budding (Aguilaniu et al., 2003; Liu et al., 2010; Zhou et al., 2014); these cytosolic Hsp104 foci are heat-shock granules. Zhou et al. (2014) observe that Hsp104 focus formation during heat shock is blocked by the translation elongation inhibitor cycloheximide (CHX) and conclude that heat-induced aggregation requires active translation. By contrast, Jacobson et al. (2012) observe that CHX blocks Hsp104 foci during arsenite stress, but not during heat shock. We wondered whether

biochemical detection might shed useful light on the relationship between aggregation, heat-shock granules, and translation.

To study these phenomena, we treated cells with 100 µg/ml CHX for 5 min and then subjected them to either a 42°C heat shock for 30 min as in Zhou et al. (2014) or to a 46°C heat shock for 8 min. This dose of CHX attenuates formation of visible fluorescent foci by tagged Pab1 (Figures 3A and 3B). However, the cytosolic heat aggregators Yef3 and Ola1 still form some fluorescent foci in the presence of CHX (Figures 3A and 3B). Thus, translation inhibition attenuates the heat-triggered formation of foci for some, but not all, cytosolic proteins.

We also measured protein aggregation biochemically during identical heat shocks by analyzing 100,000 g pelleting particles. Pab1, Ssz1, and Yef3 all enter the 100,000 g pellet after a 46°C, 10 min heat shock, with reduced aggregation after a 42°C, 30 min shock. Surprisingly, biochemical aggregation was unaffected by CHX (Figure 3C).

The data are consistent with a model of multi-stage aggregation in which initial formation of biochemical aggregates is followed by CHX-sensitive collection of these aggregates into larger bodies visible as foci. To test this model, we progressively fractionated cell lysate first at 8,000 g × 3 min (pellet, P8, largest aggregates), then fractionated the supernatant at 20,000 g × 5 min (pellet, P20, smaller aggregates), and then fractionated the second supernatant at 100,000 g × 20 min (pellet, P100, smallest aggregates), collecting residual 100,000 g supernatant (S). Western blotting against native Pab1 showed that 75% of Pab1 remained in the supernatant from unshocked cells regardless of CHX treatment (Figures 3D and S6). In cells heat shocked for 8 min at 46°C, most Pab1 entered P8 and P100; treatment with CHX blocked formation of P8 particles and increased levels of P100 particles, as predicted (Figure 3D). Ssz1 shows the same pattern (Figure 3D), as does Yef3 (total protein gel, Figure S6).

These results support a CHX-blockable secondary assembly of aggregates into cytosolic foci, which does not affect heat-induced formation of smaller aggregates.

Translation-Related Proteins Aggregate in Coherent Groups

The heat-triggered aggregation of eIF3 and the multisynthetase complex prompted us to examine aggregation of other protein complexes involved in translation. Translation factors partition into heat aggregators and non-aggregators (Figure 4A). Assuming that aggregated translation factors are inactive, the observed aggregation of eIF2B, eIF4B/G, eEF3, or eRF1 would be individually sufficient to substantially reduce net protein synthesis (Firczuk et al., 2013).

Each stable protein complex falls into a single category: of the components of eukaryotic elongation factor 1 (eEF1), all elements of the stable subcomplex eEF1B heat aggregate, but

(C) Progressive protein aggregation quantified by proportion in the supernatant fraction (pSup) during a 46°C treatment compared to unshocked replicates (top) and with increasing 8 min shock temperature (bottom; see Table S1 for design). Protein annotations in C and D are the same; superaggregators (see text) include five nucleolar proteins.

(D) Behavior of proteins in various categories (cf. C) as a function of temperature, for 8 min, and time at 46°C.

(E) Individual proteins aggregate at different rates in response to heat; more are shown in Figure S4A. In D and E, 30°C rep 1 is shown in the time course plots, the same biological sample as the 46°C data; 30°C rep 3 is shown in the temperature course plots, the same biological sample as 37°C and 42°C, 8 min, data.

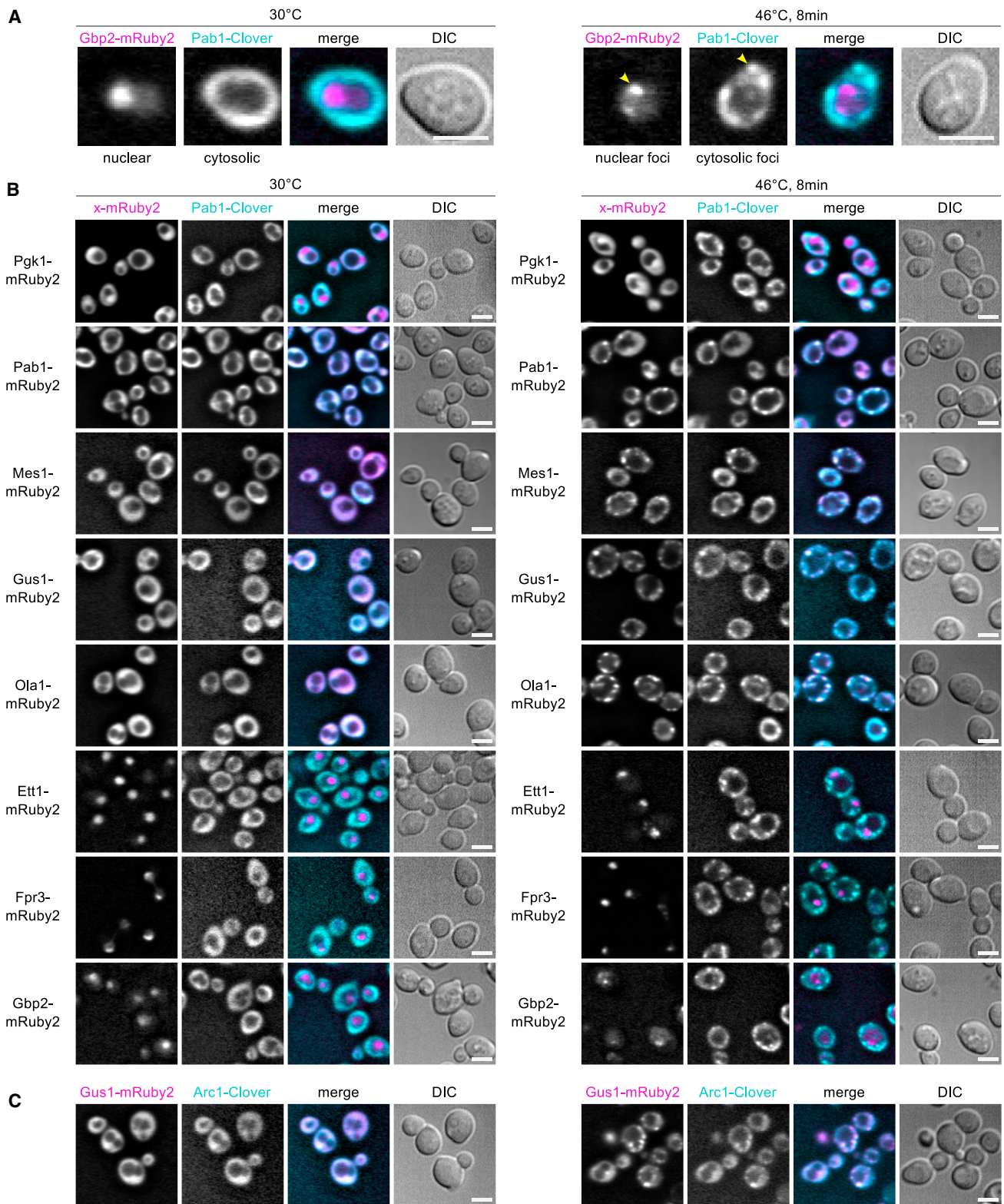


Figure 2. Live-Cell Microscopy Identifies Heat-Aggregating Proteins Forming Cytosolic or Nuclear Granules

Diploid strains containing the HSG component Pab1 tagged with the green fluorescent protein (FP) Clover (cyan in merged images) and test proteins tagged with the red FP mRuby2 (magenta in merge) were imaged at 30°C and after 8 min heat shock at 46°C. Scale bar, 5 μ m.

(legend continued on next page)

Tef1/eEF1 α does not (Figure 4A). All components of eIF2 have similar high pSup across conditions, while all components of eIF3 heat aggregate with similar kinetics (Figure 4B). Aggregation of the multisynthetase complex is particularly synchronous (Figure 4B).

Complexes with shared interaction partners show distinct aggregation patterns: for example, the nascent-polypeptide-associated complex (NAC; Egd1/Egd2) and the ribosome-associated chaperone complex (RAC; Ssz1/Zuo1), along with Ssb1/2, bind the ribosome near the nascent peptide exit tunnel (Preissler and Deuerling, 2012). Both detected NAC components remain soluble across conditions, as do ribosomes; in contrast, RAC components aggregate swiftly and in lockstep (Figure 4C). More broadly, proteins associated in annotated complexes (Pu et al., 2009) have more similar pSup trajectories than expected by chance (Figure S7).

The Yeast Multisynthetase Complex Forms Active Heat-Triggered Aggregates In Vitro

The tight correlation of the three yeast multisynthetase components during heat-triggered aggregation (Figure 4) and their aggregation into the same subcellular location (Figure 2) prompted us to ask how heat affects this complex and its activity in isolation. The complex, dubbed AME, is a heterotrimer formed by the aminoacylation cofactor Arc1 (A), methionyl-tRNA synthetase Mes1 (M), and glutamyl-tRNA synthetase Gus1 (E), which interact through eukaryote-specific N-terminal domains in each protein (Frechin et al., 2014).

Recombinant reconstituted AME remains in the supernatant of a 100,000 g, 20 min spin but after a severe 46°C 15 min treatment aggregates completely into pelletable material and cannot be resolubilized by dilution and 1 hr incubation at 30°C with or without substrates (Figure 5A).

Gentler centrifugation revealed that AME pellets as a stoichiometric complex (Figure 5A) despite wide variation in the aggregation propensity of its constituents (Figure S7C). Severely heat-shocked AME retains substantial activity, all of which resides in the aggregated fraction, as indicated by absence of activity in the supernatant after centrifugation (Figure 5B). Similarly, the activity of heat-treated Mes1 is reduced >7-fold after spinning out aggregates (Figure 5B). Gus1's non-catalytic N-terminal domain proved necessary and sufficient for heat-induced Gus1 aggregation (Figure S7D).

We next assessed the fidelity of tRNA-Met aminoacylation by AME before and after heat shock using tRNA microarrays. Under conditions in which AME is fully aggregated (cf. Figure 5A), it retains fidelity indistinguishable from untreated AME or Mes1 (Figure 5C).

Bacterial inclusion bodies can contain active exogenous enzymes (Martínez-Alonso et al., 2009). Our results reveal heat-induced formation of endogenous, active, stoichiometric aggregates with normal fidelity. Here, reduced activity may indi-

cate partial loss of function or reduced ability of large tRNA substrates to penetrate these in vitro aggregates.

Global Profiling of Disaggregation during Recovery Reveals Near-Complete Reversibility of Aggregation

Heat-shock granules slowly disappear after cells are returned to non-shock temperatures (Cherkasov et al., 2013; Parsell et al., 1994), yet it has remained unclear whether endogenous aggregate dispersion is due to disaggregation followed by degradation and resynthesis or due to disaggregation back into a stable soluble pool.

To measure disaggregation and new synthesis at the proteome scale without blocking synthesis or degradation, we performed a media-shift experiment (Figure 6A and Experimental Procedures) in which cells are grown on a first set of stable-isotope-labeled amino acids, shifted to media containing a second set of labels, then heat shocked at 42°C and allowed to recover for a defined time at 30°C. Upon collection, these cells are mixed with cells from an unshocked (30°C) reference sample grown on a third label. Supernatant fractions of these mixtures measured after 0, 20, and 60 min of recovery allowed us to observe the depletion of aggregating proteins from the supernatant after shock followed by their recovery in both the pre- and post-shock labels, indicating new synthesis, or only in the pre-shock label, indicating disaggregation.

Heat-insensitive proteins, such as the glycolytic enzyme Pgk1, show minimal change in pre-shock ratio in the supernatant, indicating no aggregation, and a slight increase in post-shock ratio, indicating low levels of new synthesis during recovery (Figure 6B). Heat-aggregating proteins have low pre-shock ratio immediately after shock, and their disaggregation is indicated by increase of the pre-shock ratio during recovery with only background-level changes in the post-shock ratio, as seen for the RNA helicase Ded1 (Figure 6B). Proteins synthesized in response to heat shock, such as the chaperone Hsp104, show an increase in both pre- and post-shock ratios, indicating new synthesis; increased signal in both channels reflects incorporation of imported post-shock amino acids and residual or recycled pre-shock amino acids (Figure 6B). Aggregated, degraded, and resynthesized proteins would show a low pre-shock ratio after shock and an increase in post-shock ratio; we do not observe this pattern.

A biological replicate with isotopic labels permuted shows the same behavior (Figure S2B). An additional time point 180 min post-shock, after a full cell doubling, shows that, as expected, the majority of the proteome incorporates the post-shock label (Figure S2C).

Proteins previously identified as superaggregators by MS aggregate aggressively at 42°C and disaggregate fully after 1 hr of recovery (Figures 6C and S4B). Complexes which aggregate coherently also disaggregate coherently, including the multisynthetase complex and the RAC (Figure 6C).

(A) Heat-induced nuclear and cytosolic aggregation of Gbp2-mRuby2 and Pab1-Clover, respectively.

(B) Non-aggregating Pgk1-mRuby2 remains diffuse during heat shock, while Pab1-Clover forms HSGs. Pab1-Clover and Pab1-mRuby2 form colocalized foci during heat shock. Fusions of MS-identified heat-aggregating proteins form foci that colocalize with Pab1 during heat shock (Mes1, Gus1, Ola1) or form sub-nuclear foci (Ett1, Fpr3, Gbp2).

(C) The aminoacylation cofactor in the multisynthetase complex, Arc1, forms heat-induced foci colocalized with Gus1.

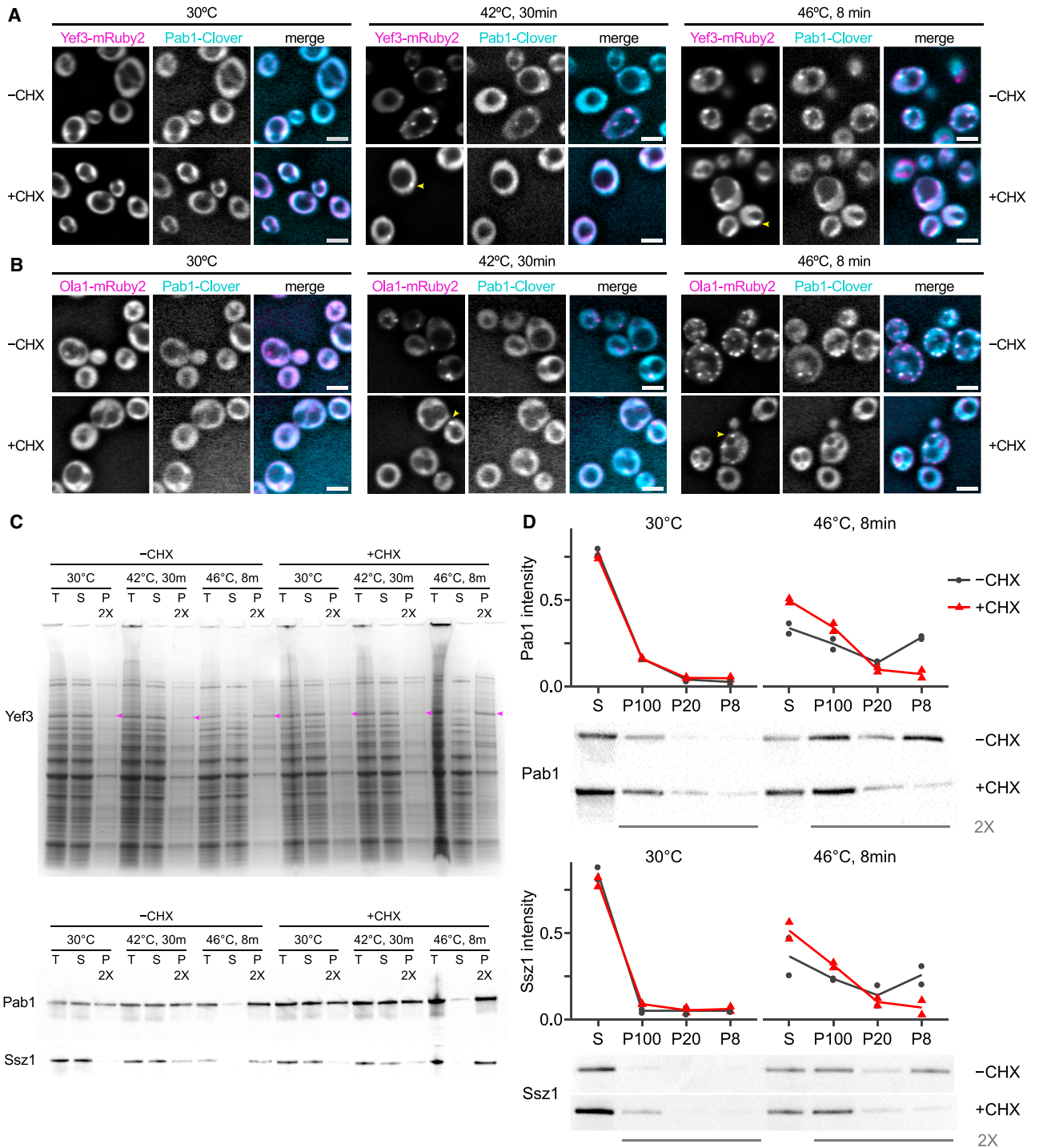


Figure 3. Heat-Triggered Protein Aggregation Does Not Require Ongoing Translation

(A) Cycloheximide (CHX; 100 μ g/ml) blocks formation of heat-triggered cytosolic foci by fluorescently tagged Pab1 and attenuates formation of foci by Yef3. Scale bars, 5 μ m; arrows indicate foci.

(B) Ola1 forms fluorescent foci in response to heat shock in the presence of CHX.

(C) Pab1, Ssz1, and Yef3 (arrows on gel) are found in the 100,000 g supernatant (S) in lysate from unshocked cells but enter the 100,000 g pellet (P) after heat shock independent of CHX treatment. Coomassie-stained protein gel and western blots against native proteins are shown. T, total protein.

(D) CHX inhibits Pab1 and Ssz1 entry into large aggregates, but not into small aggregates. Cell lysate was progressively fractionated at 8,000 g (pellet, P8), 20,000 g (P20), then 100,000 g (P100), and pellets and residual supernatant (S) were western blotted against Pab1 and Ssz1; intensity as proportion of total was quantified in two biological replicates (Figure S6), and a representative blot is shown.

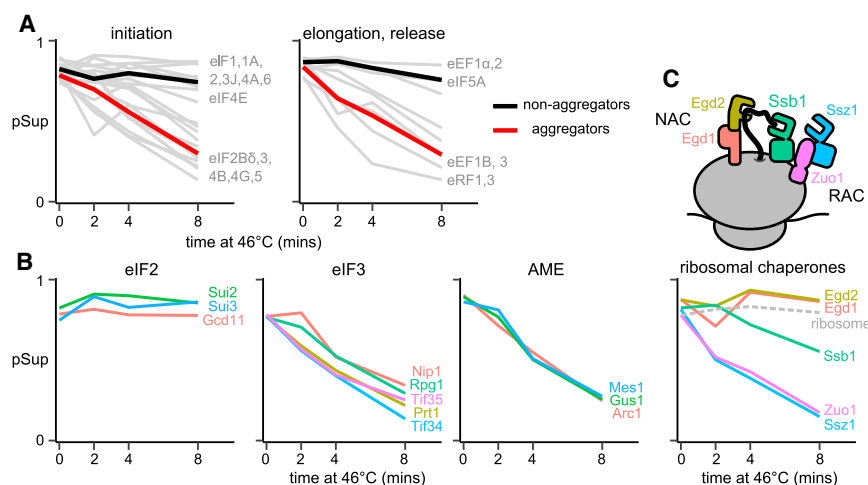


Figure 4. Stable Translation-Related Complexes Aggregate Coherently

Proportion in supernatant (pSup) is plotted against time of heat shock at 46°C; each panel shows one or more complexes and each line a protein component.

(A) pSup of all well-detected translation factors. Mean is shown for aggregators and non-aggregators in each plot.

(B) Aggregation of translation initiation factors 2 and 3 and of the multi-tRNA-synthetase complex. (C) Aggregation of chaperone complexes involved in co-translational folding.

cellular foci, and degradation—are in many cases completely separable and thus causally unrelated for endogenous mature eukaryotic proteins under acute stress. The standard misfolding model

incompletely describes the behavior of most mature proteins during heat shock.

To illustrate, consider the aggressive yet fully reversible thermally induced aggregation of nuclear proteins, exemplified by Ett1 and Gbp2, in light of recent studies on nuclear quality control. The ubiquitin ligase San1 targets nuclear misfolded proteins for degradation (Gardner et al., 2005; Fredrickson et al., 2013). GFP constructs engineered with stretches of hydrophobic residues that promote formation of fluorescent nuclear foci and pelletable aggregates undergo San1-mediated degradation detectable within 1 hr (Fredrickson et al., 2013). Our expectation was that endogenous nuclear proteins that aggregate should be similarly degraded. However, despite aggressive aggregation of Ett1 and Gbp2 in the nucleus, they are restored to solubility without degradation.

The organized deposition of aggregated proteins into particular subcellular sites, such as stress granules, may provide fitness benefits to organisms during stress (Miller et al., 2015b). Stress granules may facilitate preferential translation of certain mRNAs during stress (Kedersha and Anderson, 2002). By providing a view into how proteins reversibly form large assemblies during stress, without necessary restriction to granular structures or particular sites, our study reveals a separate layer of phenomena that is rich with exciting functional possibilities. We hypothesize that the heat-induced aggregation of mature proteins reflects the action of a vast, fast-acting regulatory system based on massive molecular assembly and disassembly. This system couples rapid protein-autonomous stress-responsive assembling elements with slower-acting disassembly machines.

Such a system invokes transient interactions beyond quaternary structure, termed quinary organization (McConkey, 1982). Molecular mechanisms and components of quinary regulation may include multivalent interactions (Li et al., 2012), low-complexity sequences (Kato et al., 2012), and phase-separation phenomena, including protein and protein/RNA liquids (Weber and Brangwynne, 2012) and hydrogels (Kato et al., 2012). Our studies do not offer a mechanistic picture of aggregation or new evidence for particular physical states of quinary assemblies but do identify targets for study.

To examine proteome-scale trends, we compared groups of genes identified as reliably soluble, heat aggregators, or superaggregators in the 46°C heat-shock data set. Immediately after heat shock, aggregators and superaggregators synthesized from pre-shock amino acids are depleted from the supernatant compared to reliable soluble proteins (Figure 6D). After 20 min recovery at 30°C, the differences between these populations are smaller though still significant, and after 60 min of recovery, the distributions are indistinguishable, indicating complete disaggregation (Figure 6D). The post-shock ratios of aggregators and superaggregators are indistinguishable from those of reliably soluble proteins, indicating approximately the same level of new synthesis. At the same time, proteins whose ribosome occupancy increases at least 20-fold during heat shock (Gerashchenko and Gladyshev, 2014) show a substantial increase in new protein synthesis (Figure 6D). New synthesis post shock correlates well with ribosome occupancy during shock (Figure S2D).

In summary, the data show virtually complete disaggregation of endogenous aggregated proteins during recovery without elevated levels of degradative turnover.

DISCUSSION

The standard model of heat stress holds that heat causes protein damage and misfolding, disrupting function and causing exposure of natively buried hydrophobic residues, which triggers protein aggregation (Vabulas et al., 2010). This model was shaped by, and explains well, a wide array of observations, particularly the behavior of endogenous nascent polypeptides. A more recent regulatory interpretation holds that evolutionarily conserved heat-induced aggregation of some proteins into specific subcellular locations reflects a mechanism for attenuating translation (Grousl et al., 2009; Farny et al., 2009; Cherkasov et al., 2013) and protecting the cell during stress (Miller et al., 2015b).

Our study provides multiple lines of evidence indicating that many phenomena that correlate tightly for nascent polypeptides and exogenous unstable reporter constructs—phenomena such as heat-induced aggregation, loss of function, formation of sub-

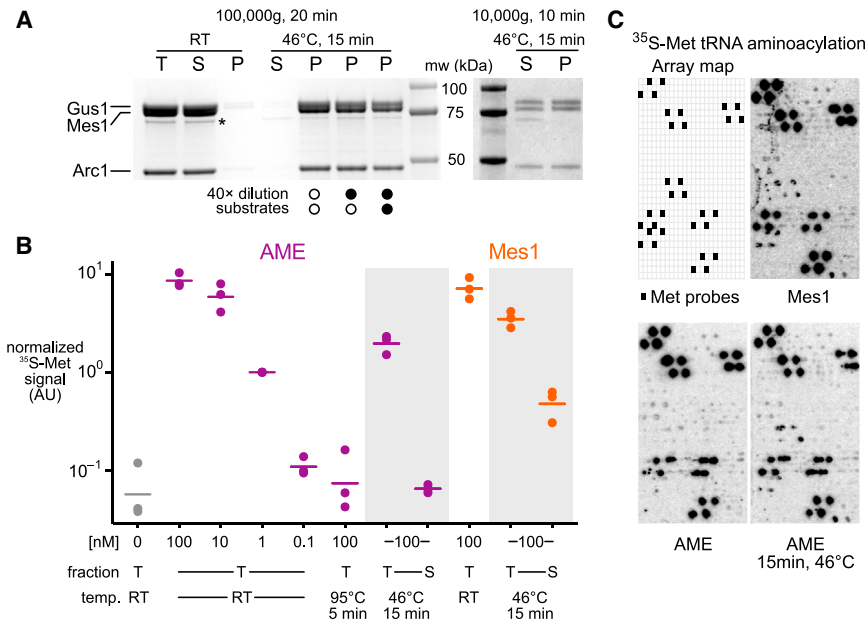


Figure 5. The Yeast Multisynthetase Complex Forms Active Aggregates in Response to Heat Shock In Vitro

(A) Recombinant purified AME complex is soluble before heat treatment and fully aggregated after (stained SDS PAGE; T, total; S, supernatant; P, pellet). A minor soluble degradation product is starred. Three heat-treated samples were incubated at room temperature (RT) for 1 hr (undiluted) or incubated for 1 hr at 30°C after 40 × dilution and after addition of substrates as indicated (see [Experimental Procedures](#)). (Right) Stoichiometry in aggregates revealed by lower-speed centrifugation. mw, molecular weight marker. (B) Activity measured by aminoacylation of total yeast tRNA with ³⁵S-labeled methionine in a filter-binding assay. Three replicates are shown, with signal normalized by 1 nM AME RT levels. Lines indicate means. (C) Fidelity measured by aminoacylation of tRNA-microarray-immobilized tRNAs with ³⁵S-labeled methionine. Each cell contains probes complementary to a single tRNA species, with tRNA-Met probes arrayed as indicated.

Because heat stress necessarily involves an influx of thermal energy, it would be efficient for aggregation to result from evolved, thermally induced conformational changes that promote quinary interactions. Such processes could be all but indistinguishable from misfolding at the molecular level ([Sengupta and Garry, 2013](#)). The fundamental distinction is in fitness: misfolding is deleterious, whereas evolved quinary regulation is beneficial, suggesting testable and opposing predictions about the fitness consequences of blocking aggregation. We also anticipate that, as in the case of the aminoacyl-tRNA synthetases, evolved quinary interactions will be domain specific, organized, and rapidly reversible without degradation, unlike the behavior of misfolded proteins.

Our data suggest several mechanisms for focusing translation on stress-induced transcripts ([Figure 7](#)). Translation initiation on most yeast mRNAs depends upon initiation factors (eIFs) and auxiliary proteins (such as the RNA helicase Ded1). We find that these factors partition into two major classes, the heat-resistant factors (including eIF-1, 1A, 2) and heat-sensitive factors (including eIF-2B, 3, 4G, 5, Ded1). [Shirokikh and Spirin \(2008\)](#) demonstrated assembly of a normal AUG-associated translation initiation complex on uncapped mRNA in vitro in the absence of eIF-2B/3/4A/4B/4G/4E if a poly(A) leader sequence is present. This poly(A)-mediated cap-independent initiation mechanism may explain the cap-independent translation of heat-shock mRNAs ([Rhoads and Lamphear, 1995](#); [Barnes et al., 1995](#); [Gerstel et al., 1992](#)), which often possess unstructured, A-rich 5' UTRs ([Holmgren et al., 1981](#)) with reduced dependence on RNA unwinding ([Lindquist and Petersen, 1990](#)). We hypothesize that stress-sensitive aggregation of initiation and unwinding factors inhibits translation on most non-stress-relevant mRNAs.

The enzyme components of the AME complex, the aminoacyl-tRNA synthetases Mes1 and Gus1, have secondary transcriptional and translational activities in the nucleus and mitochondria, respectively, and are excluded from these compartments

by complexing with Arc1 ([Frechin et al., 2014](#)). We hypothesize that autonomous heat-sensitive self-assembly of AME complexes discovered here confines active AME components to the cytosol, suppressing secondary activities in other compartments and focusing aminoacylation activity in the cytosol, where it is needed during stress ([Figure 7](#)).

Molecular chaperones may act as regulatory disassembly factors quite separate from their role in protein folding and misfolding. For example, chaperone-mediated dissolution of AME assemblies would permit return of Gus1 and Mes1 to duty in other cellular compartments. Chaperone-mediated restoration of helicases and cap-dependent initiation factors to solubility would derepress translation of most mRNAs, titrating translational activity away from stress-induced messages and thus closing a feedback loop ([Figure 7](#)). Consistent with this, deletion of the disaggregase Hsp104 delays both heat-shock granule dissolution and reassembly of polysomes after heat shock ([Cherkasov et al., 2013](#)). Which factors (chaperones or other proteins) disassemble which assemblies, and whether and how specificity is achieved, can be addressed in large part using the methods that we have introduced here.

A similar autoregulatory mechanism has been proposed as a way to link protein quality control and translation through assembly of stress granules ([Cherkasov et al., 2013](#)). Our study suggests that neither misfolding nor stress-granule formation need be involved; indeed, heat stress/aggregation/chaperones seem likely to be a special case of a broader class of signal/assembly/disassembly regulatory systems, each involving stress-specific quinary interactions. It seems likely that certain proteins will form assemblies under a wide range of stress conditions (e.g., translation initiation factors) but by stress-specific mechanisms, such as binding sites revealed by phosphorylation, pH-driven self-association, and thermally induced local unfolding. Stress-triggered formation of massive but unanchored assemblies of undamaged proteins, when reversible by stress-induced

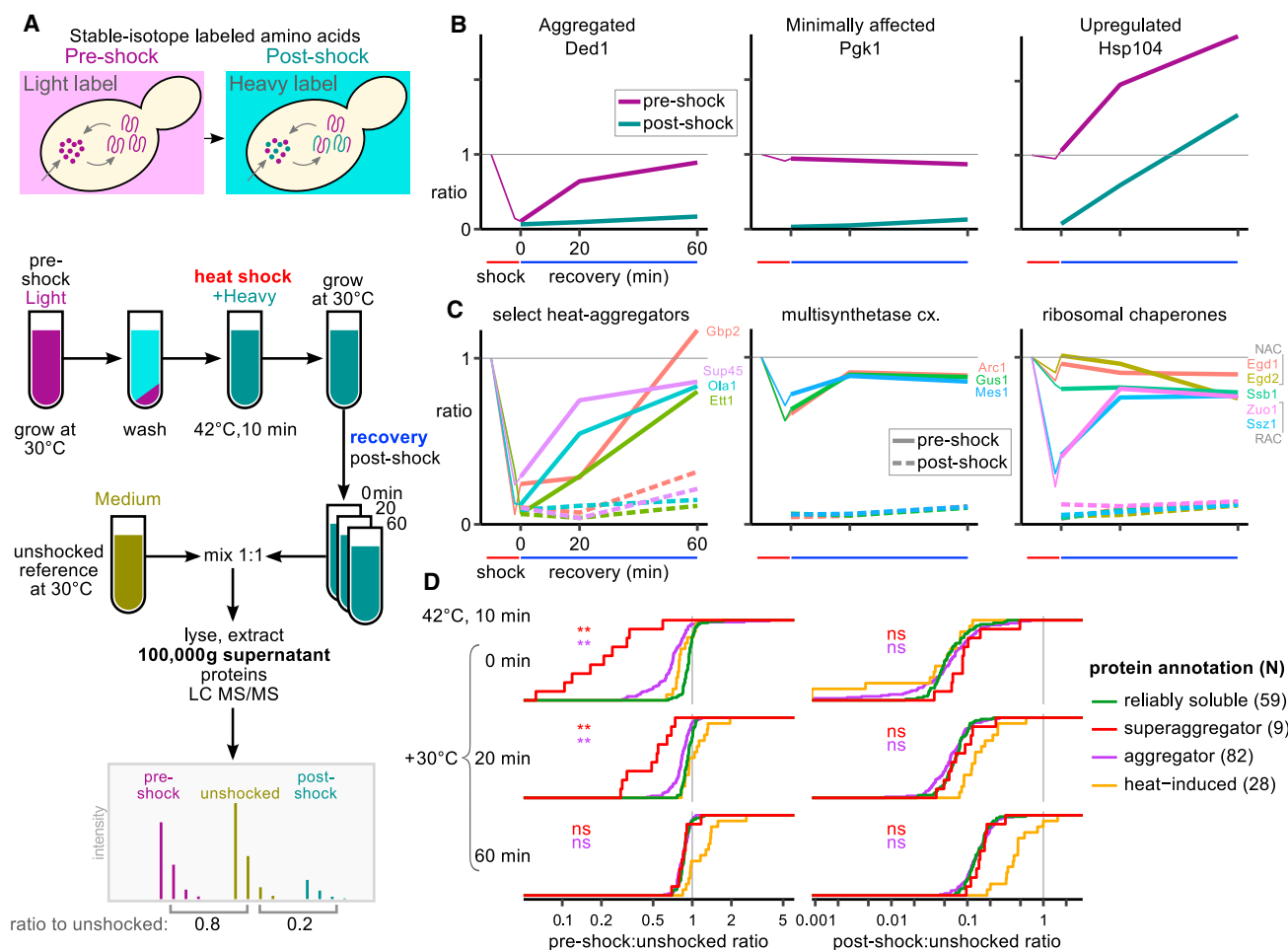


Figure 6. Heat-Aggregated Proteins Disaggregate during Recovery

(A) Schematic experimental design for SILAC media-shift measurement of soluble protein dynamics during recovery from heat shock.

(B) SILAC ratios measure aggregation or synthesis of example protein dynamics during recovery from heat shock. Thin lines show pSup after 42°C, 8 min. heat shock from Figure 1.

(C) Select groups of heat-aggregating proteins during recovery after heat shock (others in Figure S4B).

(D) Heat-aggregated proteins disaggregate during recovery, while many proteins change minimally and known heat-induced proteins are synthesized. Cumulative distributions of the normalized ratio in the supernatant are plotted for reliably soluble proteins, superaggregators, other heat aggregators (annotated in the 46°C time course), and proteins whose ribosome occupancy increases at least 20-fold during 42°C, 20 min heat shock (Gerashchenko and Gladyshev, 2014). Wilcoxon rank sum test was used to compare the distributions of reliably soluble proteins to superaggregators and other aggregators, respectively, at each time point (**p < 0.001; ns, not significant).

disassembly activity, allows for a fast-acting autoregulatory response.

EXPERIMENTAL PROCEDURES

Full details are available in the Supplemental Experimental Procedures.

Yeast Strains and Media

The yeast strains used in this study are listed in Table S6. Unless otherwise stated, S288c-derived *S. cerevisiae* were grown in SC-complete at 30°C to mid-exponential phase.

Fractionation and Mass Spectrometry Measurement

Yeast were heat treated, flash frozen, and lysed. Protein from total lysate, 100,000 g × 20 min supernatant, and pellet fractions was chloroform-

methanol extracted, separately digested with trypsin using a FASP protocol (Wiśniewski et al., 2009), labeled by reductive dimethylation (Boersema et al., 2009), and mixed. Mixed samples were fractionated by anion exchange, and fractions were submitted for LC-MS/MS analysis on an Orbitrap Velos Pro (Thermo Fisher).

SILAC Recovery Assay

Yeast strains auxotrophic for arginine and lysine (RK) were grown with light (rep. 2, heavy) isotope-labeled RK at 30°C to mid-exponential phase, transferred to heavy (rep. 2, light) isotope-labeled RK, heat shocked for 10 min at 42°C, and allowed to recover at 30°C. Cells were harvested at specified times, mixed evenly with unheated cells grown in medium-isotope-labeled RK, and flash frozen. Mixed samples were lysed and fractionated, and only the supernatant fraction was chloroform-methanol extracted, trypsin digested, and submitted for LC-MS/MS.

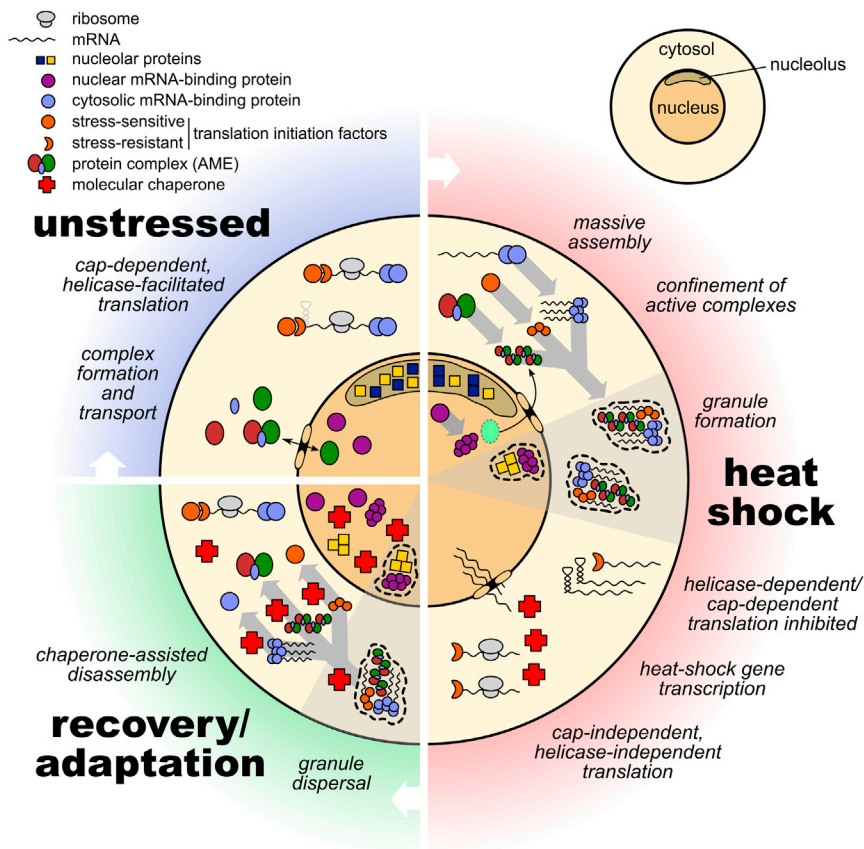


Figure 7. Mechanisms for Enhancing Cellular Remodeling by Massive Assembly during Heat Stress

request) were transformed into BY4741 and BY4742 according to standard lithium acetate protocol (Gietz and Schiestl, 2007) and selected. Two-color diploid yeast strains were constructed by crossing single-color labeled strains by standard methods.

Spinning-Disk Confocal Fluorescence Microscopy

Diploid yeast strains were imaged alive on an Olympus DSU spinning-disk confocal microscope using a 100× oil immersion objective and FITC/Cy2 and DsRed filter sets for Clover and mRuby2, respectively.

Purification of Multisynthetase Complex

Recombinant 6 × His-tagged Arc1, Gus1, and Mes1 were overexpressed, separately, in *E. coli* strain BL21 (DE3) and purified.

Aminoacylation Assay

Filter-based aminoacylation reactions and aminoacylation reactions for microarray analysis were performed as previously described (Netzer et al., 2009; Wiltrout et al., 2012).

Data Access

Raw mass spectrometry data are available on Chorus (<https://chorusproject.org>, project 753, experiments 1751 and 1752); processed data and analysis scripts are available on Dryad (<http://dx.doi.org/10.5061/dryad.hn16c>). Interactive data visualizations related to Figures 1 and 6 may be found at <http://drummondlab.org/indigenous-aggregates>.

SUPPLEMENTAL INFORMATION

Supplemental Information includes Supplemental Experimental Procedures, seven figures, and six tables and can be found with this article online at <http://dx.doi.org/10.1016/j.cell.2015.08.041>.

AUTHOR CONTRIBUTIONS

D.A.D., M.F.D., and E.W.J.W. designed the mass spectrometry experiments. E.W.J.W. and B.A.B. prepared samples for mass spectrometry, and B.A.B. obtained mass spectra. A.M.F., E.M.A., E.W.J.W., and D.A.D. designed and implemented data analysis. M.F.D., J.L.K.-S., A.E.R., and C.D.K. constructed yeast strains. J.L.K.-S. performed *in vivo* microscopy. E.W.J.W. ran western blots. E.V.P., P.R.L., J.A.R., A.E.R., and J.L.K.-S. purified proteins. E.V.P., M.H.S., P.R.L., J.A.R., T.P., and D.A.D. designed and performed multisynthetase experiments. D.A.D. and E.W.J.W. wrote the manuscript with the assistance and approval of all authors.

ACKNOWLEDGMENTS

We thank members of the Drummond lab for critical comments on the manuscript. This work was funded by grants from the Alfred P. Sloan Foundation to D.A.D. and E.M.A., the National Institutes of Health (GM105816 via the Protein Translation Research Network, and GM096193), and the Pew Charitable Trusts. D.A.D. is a Pew Scholar in the Biomedical Sciences. Imaging was performed at the University of Chicago Integrated Light Microscopy Facility; we

Data Analysis for Mass Spectrometry

Mass spectrometry runs were analyzed with MaxQuant (Cox et al., 2011), and reported peptide intensities were further analyzed using a statistical model. In brief, three intensities per peptide detection event—light, medium, and heavy—are noisy proxies for abundance in total, supernatant, and pellet, respectively. A Bayesian model, accounting for supernatant-to-total ratios, pellet-to-total ratios, variability in sample mixing, and measurement error, reports the proportion in supernatant for each detected protein.

In the SILAC recovery assay, we report median ratios of MaxQuant-estimated intensities, correcting for deviations from even mixing by fixing the median ratio to 1 for proteins reliably in the supernatant (section S1.5).

We define a protein as heat aggregating if it is (1) well-detected, i.e., two or more unique peptides reported at each time point; (2) moves consistently from supernatant to pellet, i.e., the rank correlation of pSup with time is at least 0.8; (3) moves substantially, i.e., pSup across the time course declines by at least 0.3. Superaggregating proteins are defined as the subset of heat aggregators for which pSup declines more than the most extreme HSG component at 2 min at 46°C (Tif4632, ΔpSup = 0.40).

Gene ontology (GO) enrichment analyses were performed using the topGO package (Alexa et al., 2006).

Protein Gel Electrophoresis and Western Blotting

SDS-PAGE was performed according to standard methods. Proteins were transferred to nitrocellulose membranes, detected with antibodies against Pab1 (EnCor; #MCA-1G1) or Ssz1 (Hundley et al., 2002), and visualized by chemiluminescence.

Generation of Diploid Yeast Strains

Plasmids pJLS033 and pJLS035 were constructed for C-terminal Clover and mRuby2 labeling at the native locus. Clover/mRuby2 KanMX cassette PCR fragments generated by unique primer pairs (sequences provided upon

thank V. Bindokas and C. Labno for their help. We thank B. Glick and K. Day for assistance with image processing, E. Craig for the generous gift of the Ssz1 antibody, Y. Gilad and B. Engelmann for use of computing resources, J. Piccirilli and B. Weissman for scintillation counting assistance, and T. Sosnick for assistance with absorbance and scattering measurements. Some computations were run on the Odyssey cluster supported by the FAS Division of Science, Research Computing Group at Harvard University.

Received: April 1, 2015

Revised: June 19, 2015

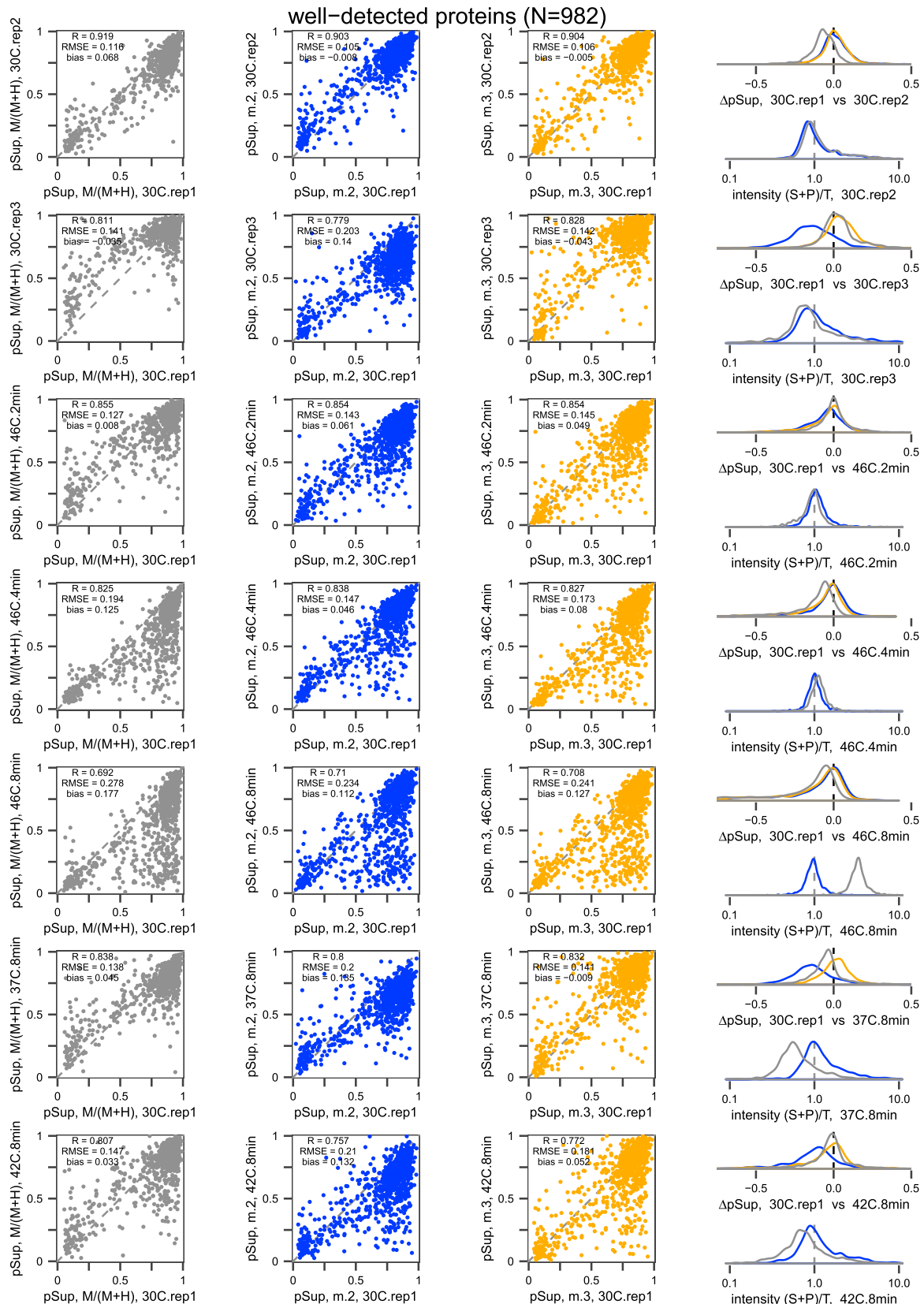
Accepted: August 5, 2015

Published: September 10, 2015

REFERENCES

- Aguilaniu, H., Gustafsson, L., Rigoulet, M., and Nyström, T. (2003). Asymmetric inheritance of oxidatively damaged proteins during cytokinesis. *Science* 299, 1751–1753.
- Alexa, A., Rahnenführer, J., and Lengauer, T. (2006). Improved scoring of functional groups from gene expression data by decorrelating GO graph structure. *Bioinformatics* 22, 1600–1607.
- Baler, R., Welch, W.J., and Voellmy, R. (1992). Heat shock gene regulation by nascent polypeptides and denatured proteins: hsp70 as a potential autoregulatory factor. *J. Cell Biol.* 117, 1151–1159.
- Barnes, C.A., MacKenzie, M.M., Johnston, G.C., and Singer, R.A. (1995). Efficient translation of an SSA1-derived heat-shock mRNA in yeast cells limited for cap-binding protein and eIF-4F. *Mol. Gen. Genet.* 246, 619–627.
- Boersema, P.J., Raijmakers, R., Lemeer, S., Mohammed, S., and Heck, A.J.R. (2009). Multiplex peptide stable isotope dimethyl labeling for quantitative proteomics. *Nat. Protoc.* 4, 484–494.
- Buchan, J.R., Nissan, T., and Parker, R. (2010). Analyzing P-bodies and stress granules in *Saccharomyces cerevisiae*. *Methods Enzymol.* 470, 619–640.
- Buchan, J.R., Yoon, J.-H., and Parker, R. (2011). Stress-specific composition, assembly and kinetics of stress granules in *Saccharomyces cerevisiae*. *J. Cell Sci.* 124, 228–239.
- Buchan, J.R., Kolaitis, R.-M., Taylor, J.P., and Parker, R. (2013). Eukaryotic stress granules are cleared by autophagy and Cdc48/VCP function. *Cell* 153, 1461–1474.
- Cherkasov, V., Hofmann, S., Druffel-Augustin, S., Mogk, A., Tyedmers, J., Stoecklin, G., and Bukau, B. (2013). Coordination of translational control and protein homeostasis during severe heat stress. *Curr. Biol.* 23, 2452–2462.
- Cherry, J.M., Hong, E.L., Amundsen, C., Balakrishnan, R., Binkley, G., Chan, E.T., Christie, K.R., Costanzo, M.C., Dwight, S.S., Engel, S.R., et al. (2012). *Saccharomyces Genome Database: the genomics resource of budding yeast*. *Nucleic Acids Res.* 40, D700–D705.
- Cox, J., Neuhauser, N., Michalski, A., Scheltema, R.A., Olsen, J.V., and Mann, M. (2011). Andromeda: a peptide search engine integrated into the MaxQuant environment. *J. Proteome Res.* 10, 1794–1805.
- Farny, N.G., Kedersha, N.L., and Silver, P.A. (2009). Metazoan stress granule assembly is mediated by P-eIF2 α -dependent and -independent mechanisms. *RNA* 15, 1814–1821.
- Firczuk, H., Kannambath, S., Pahle, J., Claydon, A., Beynon, R., Duncan, J., Westerhoff, H., Mendes, P., and McCarthy, J.E. (2013). An *in vivo* control map for the eukaryotic mRNA translation machinery. *Mol. Syst. Biol.* 9, 635.
- Frechin, M., Enkler, L., Tetaud, E., Laporte, D., Senger, B., Blancard, C., Hamann, P., Bader, G., Clauder-Münster, S., Steinmetz, L.M., et al. (2014). Expression of nuclear and mitochondrial genes encoding ATP synthase is synchronized by disassembly of a multisynthetase complex. *Mol. Cell* 56, 763–776.
- Fredrickson, E.K., Gallagher, P.S., Clowes Candadai, S.V., and Gardner, R.G. (2013). Substrate recognition in nuclear protein quality control degradation is governed by exposed hydrophobicity that correlates with aggregation and insolubility. *J. Biol. Chem.* 288, 6130–6139.
- Gardner, R.G., Nelson, Z.W., and Gottschling, D.E. (2005). Degradation-mediated protein quality control in the nucleus. *Cell* 120, 803–815.
- Gerashchenko, M.V., and Gladyshev, V.N. (2014). Translation inhibitors cause abnormalities in ribosome profiling experiments. *Nucleic Acids Res.* 42, e134.
- Gerstel, B., Tuite, M.F., and McCarthy, J.E.G. (1992). The effects of 5'-capping, 3'-polyadenylation and leader composition upon the translation and stability of mRNA in a cell-free extract derived from the yeast *Saccharomyces cerevisiae*. *Mol. Microbiol.* 6, 2339–2348.
- Gietz, R.D., and Schiestl, R.H. (2007). High-efficiency yeast transformation using the LiAc/SS carrier DNA/PEG method. *Nat. Protoc.* 2, 31–34.
- Glover, J.R., and Lindquist, S. (1998). Hsp104, Hsp70, and Hsp40: a novel chaperone system that rescues previously aggregated proteins. *Cell* 94, 73–82.
- Grousl, T., Ivanov, P., Frýdlová, I., Vasicová, P., Janda, F., Vojtová, J., Malinská, K., Malcová, I., Nováková, L., Janosková, D., et al. (2009). Robust heat shock induces eIF2 α -phosphorylation-independent assembly of stress granules containing eIF3 and 40S ribosomal subunits in budding yeast, *Saccharomyces cerevisiae*. *J. Cell Sci.* 122, 2078–2088.
- Grousl, T., Ivanov, P., Malcova, I., Pompach, P., Frydlova, I., Slaba, R., Senohrabkova, L., Novakova, L., and Hasek, J. (2013). Heat shock-induced accumulation of translation elongation and termination factors precedes assembly of stress granules in *S. cerevisiae*. *PLoS ONE* 8, e57083.
- Heck, J.W., Cheung, S.K., and Hampton, R.Y. (2010). Cytoplasmic protein quality control degradation mediated by parallel actions of the E3 ubiquitin ligases Ubr1 and San1. *Proc. Natl. Acad. Sci. USA* 107, 1106–1111.
- Holmgren, R., Corces, V., Morimoto, R., Blackman, R., and Meselson, M. (1981). Sequence homologies in the 5' regions of four *Drosophila* heat-shock genes. *Proc. Natl. Acad. Sci. USA* 78, 3775–3778.
- Hundley, H., Eisenman, H., Walter, W., Evans, T., Hotokezaka, Y., Wiedmann, M., and Craig, E. (2002). The *in vivo* function of the ribosome-associated Hsp70, Ssz1, does not require its putative peptide-binding domain. *Proc. Natl. Acad. Sci. USA* 99, 4203–4208.
- Jacobson, T., Navarrete, C., Sharma, S.K., Sideri, T.C., Ibstedt, S., Priya, S., Grant, C.M., Christen, P., Goloubinoff, P., and Tamás, M.J. (2012). Arsenite interferes with protein folding and triggers formation of protein aggregates in yeast. *J. Cell Sci.* 125, 5073–5083.
- Kato, M., Han, T.W., Xie, S., Shi, K., Du, X., Wu, L.C., Mirzaei, H., Goldsmith, E.J., Longgood, J., Pei, J., et al. (2012). Cell-free formation of RNA granules: low complexity sequence domains form dynamic fibers within hydrogels. *Cell* 149, 753–767.
- Kedersha, N., and Anderson, P. (2002). Stress granules: sites of mRNA triage that regulate mRNA stability and translatability. *Biochem. Soc. Trans.* 30, 963–969.
- Lam, A.J., St-Pierre, F., Gong, Y., Marshall, J.D., Cranfill, P.J., Baird, M.A., McKeown, M.R., Wiedenmann, J., Davidson, M.W., Schnitzer, M.J., et al. (2012). Improving FRET dynamic range with bright green and red fluorescent proteins. *Nat. Methods* 9, 1005–1012.
- Li, P., Banjade, S., Cheng, H.C., Kim, S., Chen, B., Guo, L., Llaguno, M., Hollingsworth, J.V., King, D.S., Banani, S.F., et al. (2012). Phase transitions in the assembly of multivalent signalling proteins. *Nature* 483, 336–340.
- Lindquist, S. (1986). The heat-shock response. *Annu. Rev. Biochem.* 55, 1151–1191.
- Lindquist, S., and Petersen, R. (1990). Selective translation and degradation of heat-shock messenger RNAs in *Drosophila*. *Enzyme* 44, 147–166.
- Liu, B., Larsson, L., Caballero, A., Hao, X., Oling, D., Grantham, J., and Nyström, T. (2010). The polarisome is required for segregation and retrograde transport of protein aggregates. *Cell* 140, 257–267.
- Martínez-Alonso, M., González-Montalbán, N., García-Fruitós, E., and Villaverde, A. (2009). Learning about protein solubility from bacterial inclusion bodies. *Microb. Cell Fact.* 8, 4.
- McConkey, E.H. (1982). Molecular evolution, intracellular organization, and the quinary structure of proteins. *Proc. Natl. Acad. Sci. USA* 79, 3236–3240.

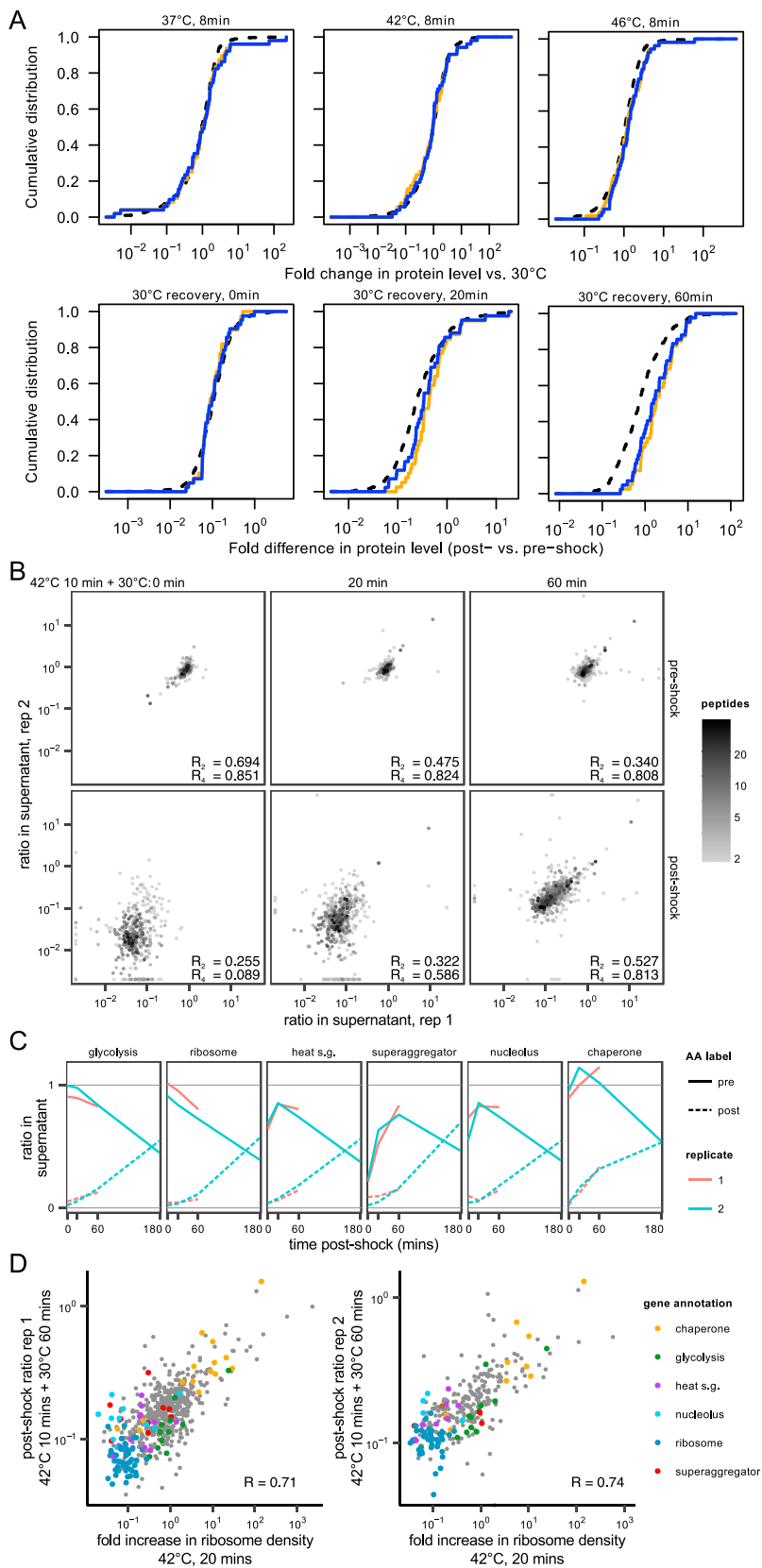
- Medicherla, B., and Goldberg, A.L. (2008). Heat shock and oxygen radicals stimulate ubiquitin-dependent degradation mainly of newly synthesized proteins. *J. Cell Biol.* *182*, 663–673.
- Miller, S.B., Ho, C.-T., Winkler, J., Khokhrina, M., Neuner, A., Mohamed, M.Y., Guilbride, D.L., Richter, K., Lisby, M., Schiebel, E., et al. (2015a). Compartment-specific aggregates direct distinct nuclear and cytoplasmic aggregate deposition. *EMBO J.* *34*, 778–797.
- Miller, S.B.M., Mogk, A., and Bukau, B. (2015b). Spatially organized aggregation of misfolded proteins as cellular stress defense strategy. *J. Mol. Biol.* *427*, 1564–1574.
- Mogk, A., Tomoyasu, T., Goloubinoff, P., Rüdiger, S., Röder, D., Langen, H., and Bukau, B. (1999). Identification of thermolabile *Escherichia coli* proteins: prevention and reversion of aggregation by DnaK and ClpB. *EMBO J.* *18*, 6934–6949.
- Netzer, N., Goodenbour, J.M., David, A., Dittmar, K.A., Jones, R.B., Schneider, J.R., Boone, D., Eves, E.M., Rosner, M.R., Gibbs, J.S., et al. (2009). Innate immune and chemically triggered oxidative stress modifies translational fidelity. *Nature* *462*, 522–526.
- Nover, L., Scharf, K.D., and Neumann, D. (1983). Formation of cytoplasmic heat shock granules in tomato cell cultures and leaves. *Mol. Cell. Biol.* *3*, 1648–1655.
- Parsell, D.A., Kowal, A.S., Singer, M.A., and Lindquist, S. (1994). Protein disaggregation mediated by heat-shock protein Hsp104. *Nature* *372*, 475–478.
- Preissler, S., and Deuring, E. (2012). Ribosome-associated chaperones as key players in proteostasis. *Trends Biochem. Sci.* *37*, 274–283.
- Pu, S., Wong, J., Turner, B., Cho, E., and Wodak, S.J. (2009). Up-to-date catalogues of yeast protein complexes. *Nucleic Acids Res.* *37*, 825–831.
- Rhoads, R., and Lamphear, B. (1995). Cap-independent translation of heat shock messenger RNAs. *Curr. Top. Microbiol. Immunol.* *203*, 131–153.
- Samanfar, B., Tan, H., Shostak, K., Chalabian, F., Wu, Z., Alamgir, M., Sunba, N., Burnside, D., Omid, K., Hooshyar, M., et al. (2014). A global investigation of gene deletion strains that affect premature stop codon bypass in yeast, *Saccharomyces cerevisiae*. *Mol. Biosyst.* *10*, 916–924.
- Sengupta, P., and Garrity, P. (2013). Sensing temperature. *Curr. Biol.* *23*, R304–R307.
- Shirokikh, N.E., and Spirin, A.S. (2008). Poly(A) leader of eukaryotic mRNA bypasses the dependence of translation on initiation factors. *Proc. Natl. Acad. Sci. USA* *105*, 10738–10743.
- Vabulas, R.M., Raychaudhuri, S., Hayer-Hartl, M., and Hartl, F.U. (2010). Protein folding in the cytoplasm and the heat shock response. *Cold Spring Harb. Perspect. Biol.* *2*, a004390.
- Verghese, J., Abrams, J., Wang, Y., and Morano, K.A. (2012). Biology of the heat shock response and protein chaperones: budding yeast (*Saccharomyces cerevisiae*) as a model system. *Microbiol. Mol. Biol. Rev.* *76*, 115–158.
- Weber, S.C., and Brangwynne, C.P. (2012). Getting RNA and protein in phase. *Cell* *149*, 1188–1191.
- Wiltrot, E., Goodenbour, J.M., Fréchin, M., and Pan, T. (2012). Misacylation of tRNA with methionine in *Saccharomyces cerevisiae*. *Nucleic Acids Res.* *40*, 10494–10506.
- Wiśniewski, J.R., Zougman, A., Nagaraj, N., and Mann, M. (2009). Universal sample preparation method for proteome analysis. *Nat. Methods* *6*, 359–362.
- Zhou, C., Slaughter, B.D., Unruh, J.R., Guo, F., Yu, Z., Mickey, K., Narkar, A., Ross, R.T., McClain, M., and Li, R. (2014). Organelle-based aggregation and retention of damaged proteins in asymmetrically dividing cells. *Cell* *159*, 530–542.



(legend on next page)

Figure S1. Statistical Models Estimate Proportion in Supernatant Reproducibly between Biological Replicates, Related to Experimental Procedures and Figure 1

For the scatter plots, each dot represents a well-detected protein, x-axes are estimates of proportion in supernatant (pSup) from unshocked (30°C) replicate 1, and y-axes are pSup estimates from other conditions and replicates. R is Pearson's correlation coefficient, RMSE is root mean squared error, bias is mean difference, in pSup between condition (as y axis) and control (30°C, rep 1). Left column (gray) naively estimates pSup as the median of the ratios $M/(M+H)$ across peptides (M, medium intensity; H, heavy intensity). Middle column (blue) estimates pSup with the Bayesian model correcting for noise and mixing variability. Right column (gold) further normalizes for dynamic range, applied to output of the Bayesian model. See [Supplemental Experimental Procedures](#) for details. Distribution plots of difference (Δ) in pSup use the same colors and data as the scatter plots. Distributions of $(S+P)/T$ compare proteinwise summed intensity on a log-scale, before (gray) or after (blue) correcting for mixing ratio using estimates from the Bayesian model.

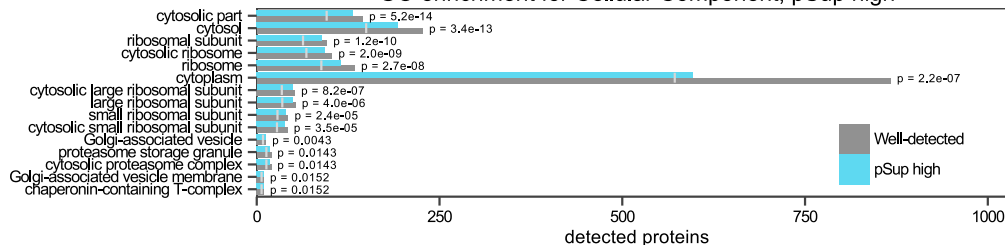


(legend on next page)

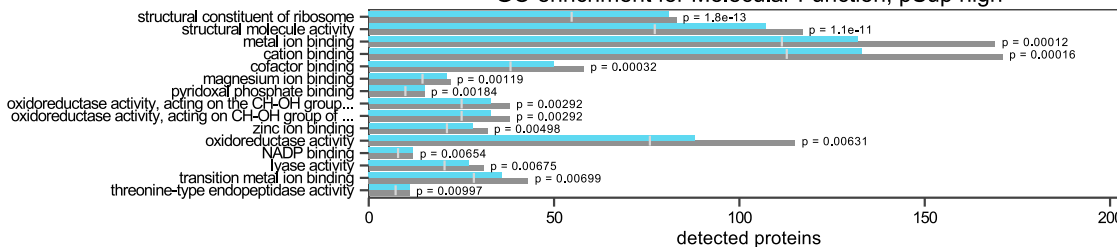
Figure S2. No Detectable Protein-Level Heat-Shock Response during 8 min Heat Shocks; Detectable Response during Recovery, Related to Figures 1 and 6

(A) Top, fold change in protein levels during 8 min treatments relative to the 30°C control. Bottom, fold difference in protein levels, comparing new synthesis to pre-shock levels, during recovery from a 10 min, 42°C shock. All comparisons show ratios of protein LC-MS/MS intensities. Dashed black line shows all well-detected proteins, orange line shows proteins from genes with at least 5-fold induced mRNAs after a 42°C, 10 min shock (Swamy et al., 2014), and blue line shows proteins from genes whose translational induction, assessed by ribosome profiling, increases by at least 5-fold after a 42°C, 20 min shock (Gerashchenko and Gladyshev, 2014). By Wilcoxon signed-rank test, all differences are insignificant ($p > 0.02$ with no multiple-testing correction) with the exception of the 60 min recovery time point, where both transcriptional and translationally upregulated genes are also induced at the protein level in our study ($p < 10^{-4}$). (B) Ratios in supernatant for pre-shock and post-shock labeled amino acids at all time points measured in both datasets; Pearson correlation coefficients (R) are shown filtered by minimum number of peptides detected per protein (2 or 4), and points are shaded by minimum number of peptides detected, starting with 2. The higher dispersion and lower correlation for proteins with fewer detected peptides indicates that much of the dispersion is due to measurement noise in peptide detections. (C) Median trajectories of ratios for protein groups in replicates of recovery dataset. (D) New protein synthesis, as measured by post-shock:unshocked amino acid ratio in supernatant, correlates with increased ribosome occupancy measured by Gerashchenko and Gladyshev (2014), for both replicates. Proteins are filtered to be well-detected in the recovery dataset (2 or more unique peptides detected per protein) and in the ribosome occupancy dataset ($\text{rpkm} \geq 10$ in shocked and unshocked samples), and outliers Nnt1 and Vps4 are excluded from the plots, but included in the correlation coefficient.

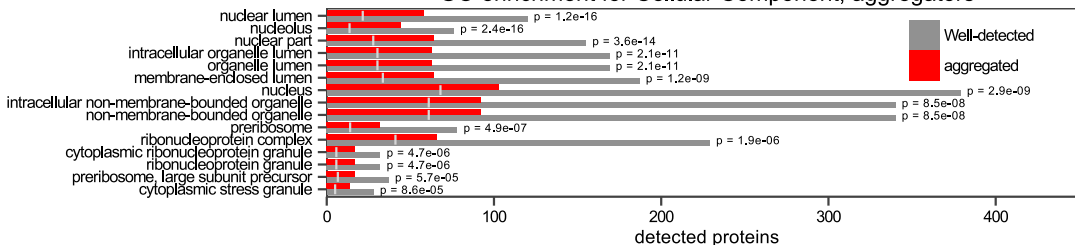
GO enrichment for Cellular Component, pSup high



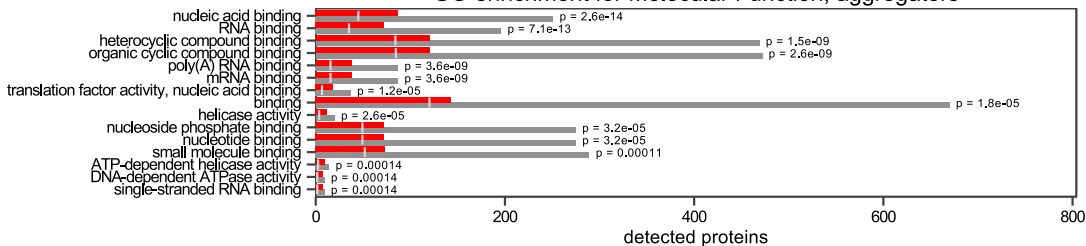
GO enrichment for Molecular Function, pSup high



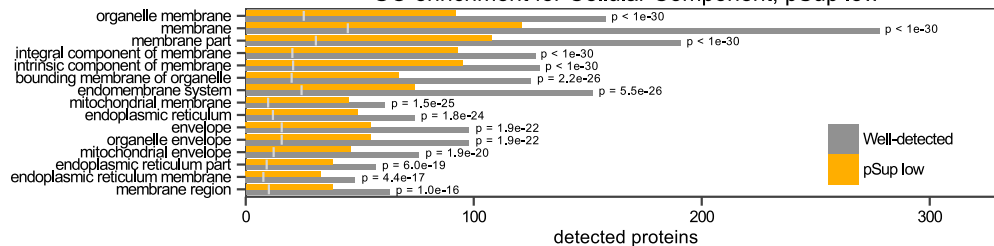
GO enrichment for Cellular Component, aggregators



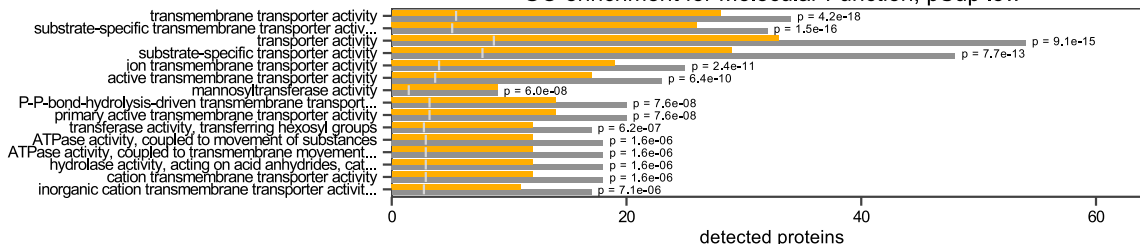
GO enrichment for Molecular Function, aggregators



GO enrichment for Cellular Component, pSup low



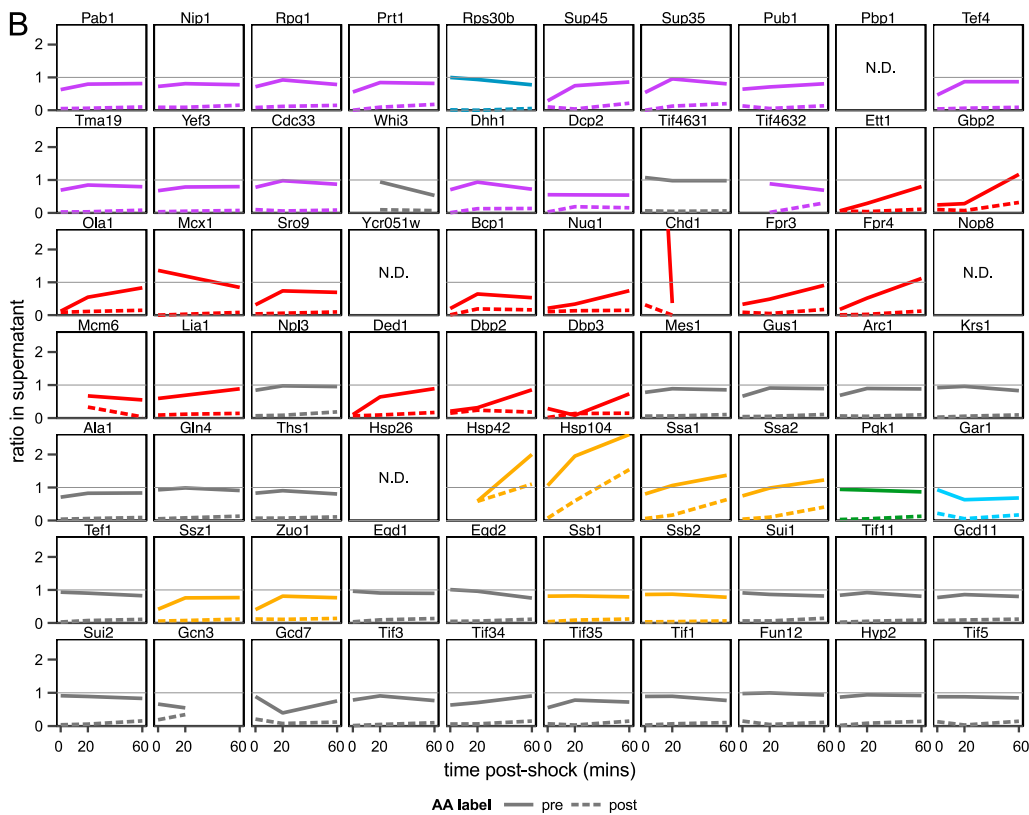
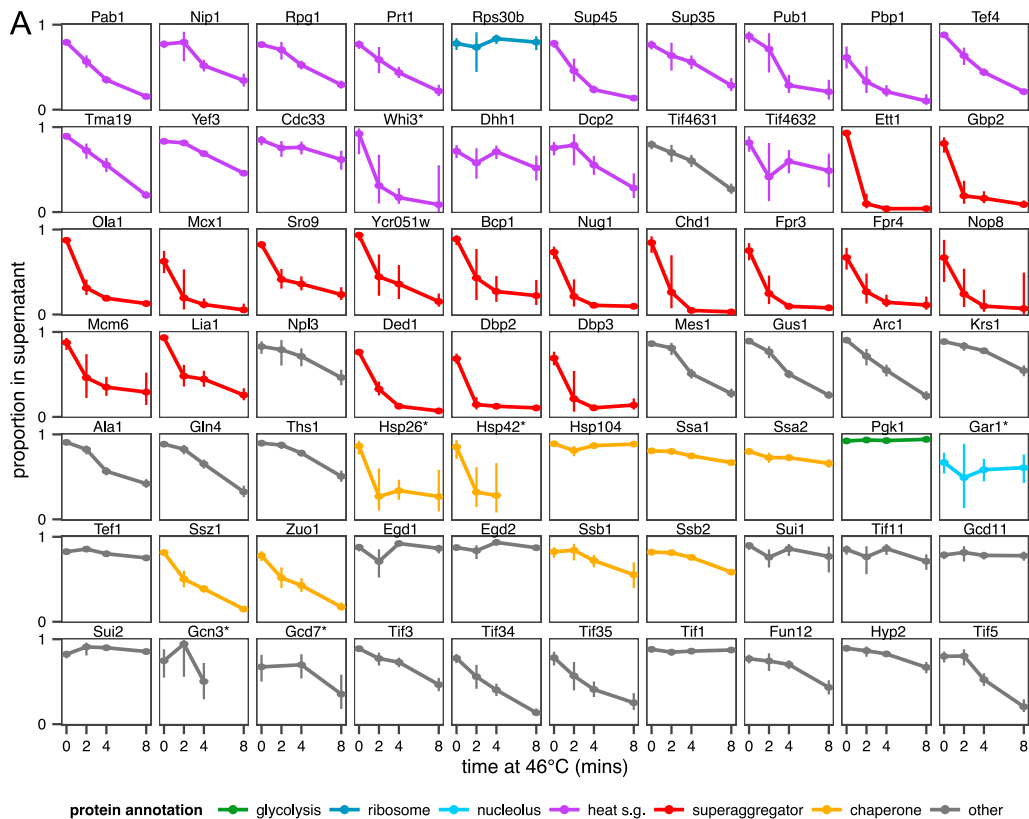
GO enrichment for Molecular Function, pSup low



(legend on next page)

Figure S3. Gene Ontology Terms Enriched in High and Low pSup Proteins and Heat-Aggregating Proteins, Related to Figure 1

Enrichment analyses were performed to test which gene ontology (GO) terms were enriched in proteins with high and low pSup, compared to the null expectation of random binomial assignment (gray vertical line). High pSup are those well-detected proteins with mean pSup ≥ 0.5 , and low pSup those with mean pSup ≤ 0.5 , excluding aggregating proteins. GO terms were taken from SGD (Cherry et al., 2012), and calculations were done using Fisher's exact test, with the topGO package (Alexa et al., 2006). Aggregating proteins were identified as described in experimental procedures.



(legend on next page)

Figure S4. Heat Aggregation and Disaggregation of Select Proteins, Related to Figure 1

(A) Proportion in supernatant (pSup) during 46°C time course is shown for proteins mentioned in the text, including heat shock granule components, superaggregators, molecular chaperones, tRNA synthetases and translation factors. Median estimate (point) and central 95% Bayesian credible interval (vertical interval) are displayed. Genes indicated by asterisk (*) are not well-detected. Fpr3 and Fpr4 are nucleolar proteins and superaggregators, here colored as superaggregators. (B) Ratios in supernatant of select proteins during recovery from heat shock. Replicate 1 is shown; data from all detected proteins, in both replicates, are included in supplemental data and are visualizable online at <http://drummondlab.org/endogenous-aggregates>. Ratio in supernatant is shown for all proteins mentioned in the results section, and all superaggregators; some proteins (e.g., Tif4632) are detected at only some time points and others (e.g., Pbp1) are not detected. The value at 0 min for Chd1 lies above the y axis limits. Fpr3 and Fpr4 are nucleolar proteins also classified as superaggregators.

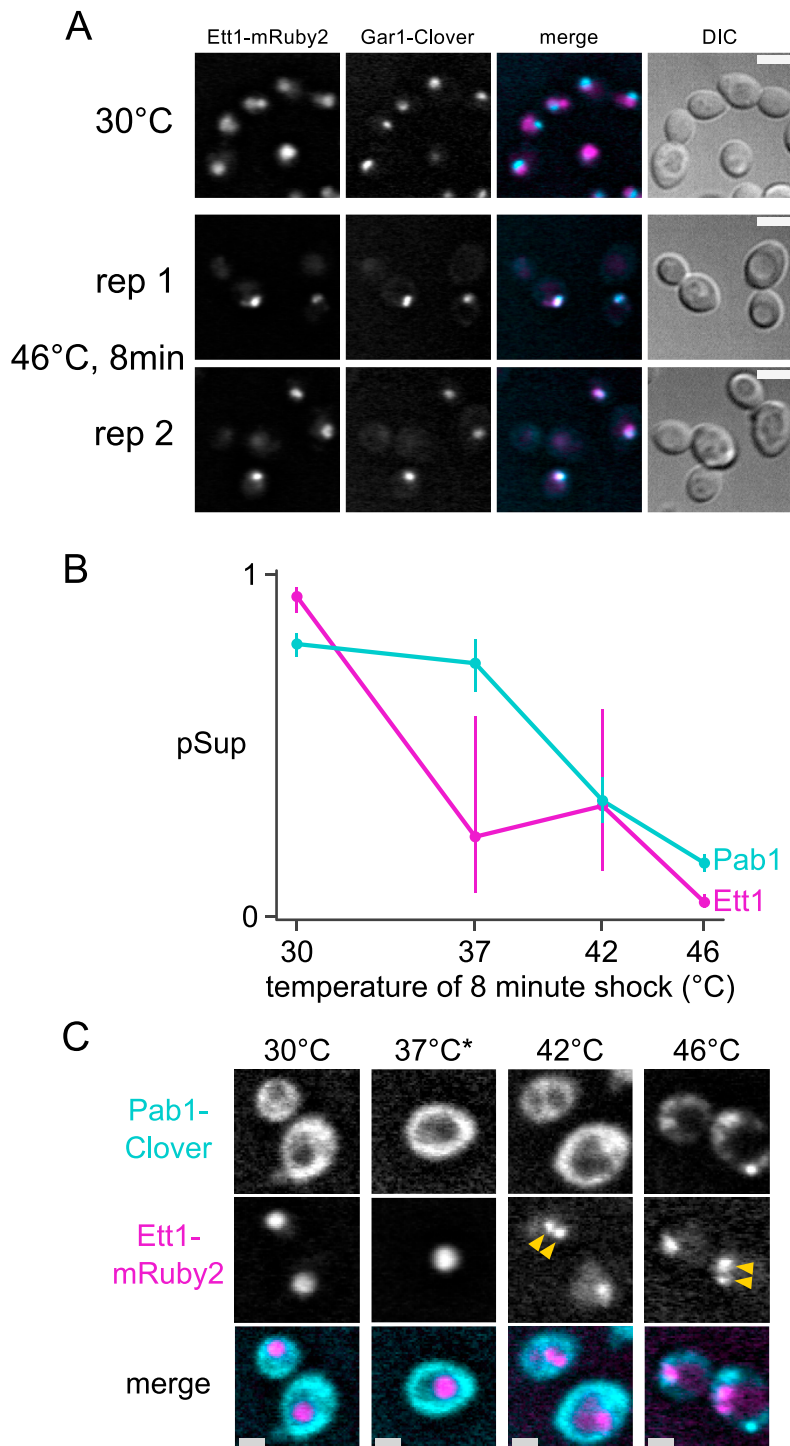


Figure S5. Ett1 Relocalizes to the Nucleolar Periphery during Heat Shock, and Its Rapid Aggregation Is Detectable without Formation of Fluorescent Foci, Related to Figures 2 and 3

(A) Ett1 and Gar1 localization converge upon heat shock. Gar1 is a nucleolar marker that does not aggregate during heat shock. Ett1-mRuby2 and Gar1-Clover fusions show distinct nuclear localization of the two proteins at 30°C, with closer association after 8 min heat shock at 46°C. Scale bar represents 5 μ m in all panels. (B) Proportion in supernatant (pSup) for Pab1 and Ett1 after an 8 min heat shock at varying temperatures; 95% credible intervals are shown. (C) Microscopy of fluorescently tagged Pab1 and Ett1 at 30°C, after 10 min (noted by *) treatment at 37°C, or 8 min treatment at 42°C or 46°C. Formation of pelletable aggregates is detected in conditions where no foci are visible, for Ett1 at 37°C, and for Pab1 at 42°C. Arrows indicate instances of multiple nuclear Ett1 foci.

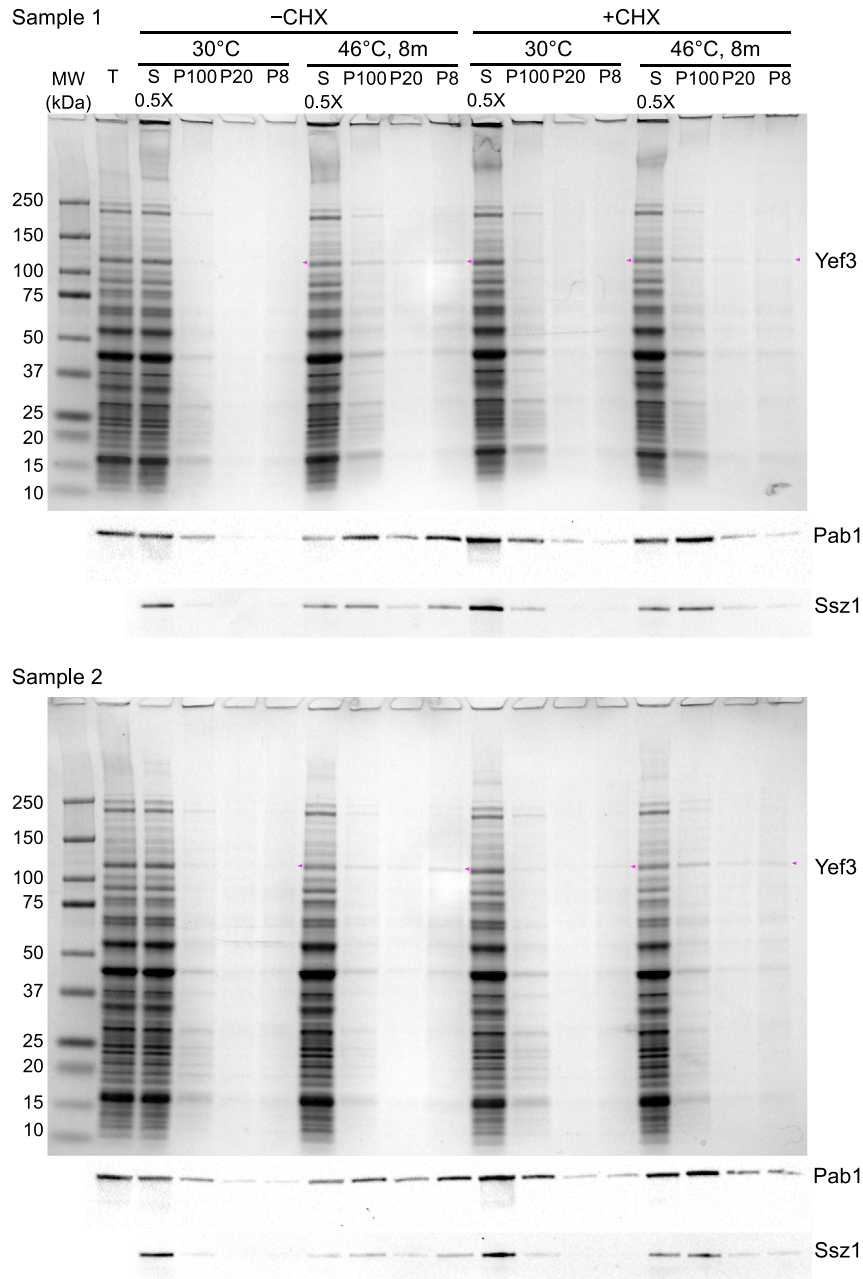


Figure S6. Heat-Triggered Protein Aggregation Does Not Require Ongoing Translation, Related to Figure 3

After 8 min at 46°C some proteins, indicated by arrows, aggregate in response to heat, regardless of cycloheximide treatment. Two biological replicates are shown of denaturing protein gel (SDS-PAGE, Coomassie stained) analysis of fractionated cell lysate, with and without heat shock, with and without 100 µg/ml cycloheximide treatment (see methods), and anti-Pab1 and anti-Ssz1 western blots from identically loaded gels (total protein sample was not loaded for Ssz1 gels). Quantification of the blots is shown in Figure 3.

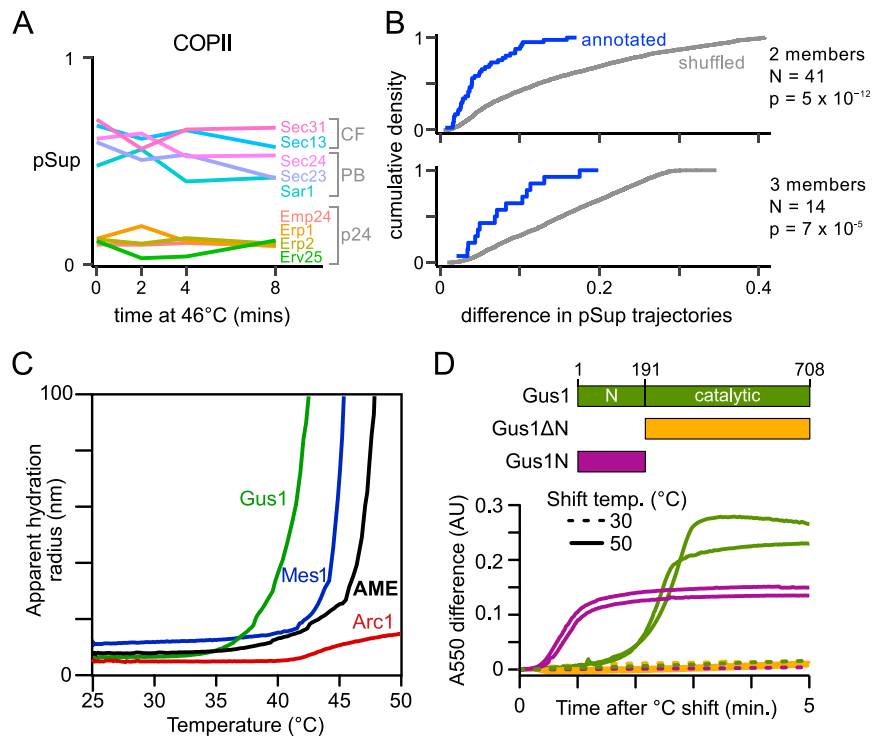


Figure S7. Complexes Coherently Aggregate and Show Component- and Domain-Specific Aggregation Propensity, Related to Figure 4

(A) The COPII coat protein complex consists of three subcomplexes, whose proportion in supernatant (pSup) tracks their degree of membrane association. The COPII complex, which transports proteins from the ER to the Golgi, consists of a constitutively membrane-associated p24 complex (Erp1, Erp2, Erp24, and Erv25), the prebudding complex (PB; Sec23/Sec24 dimer, Sar1) which initially binds the ER membrane to form a vesicle, and the remaining vesicle coat-forming (CF) Sec13/Sec31 tetramer. Across all heat shock treatments, we observed the p24 complex pelleted and the other vesicle coat proteins partially pelleted; the prebudding complex has lower pSup than the late-binding coat-forming components. (B) Proteins annotated to the same complex have similar pSup across heatshock time points. For each complex annotated in CYC2008 (Pu et al., 2009) with 2 or 3 well-detected proteins, we compute the intracomplex mean-squared distance in pSup across time points, and plot the cumulative density (blue line). As a null distribution, we sampled 2000 pairs or triplets of well detected proteins and estimate intracomplex distance in pSup (gray line). We present p-values for a one-sided Wilcoxon rank test of the hypothesis that the intracomplex distance for annotated complex is less than for randomly sampled complexes. These distributions are clearly different, despite some annotated complexes consisting of stable subcomplexes, each of which has pSup more similar to the supercomplex, as for COPII. (C) Particle size versus temperature for recombinant AME components (Arc1, A; Mes1, M; Gus1, E) and reconstituted AME complex measured by dynamic light scattering (DLS). (D) Aggregation of full-length Gus1 and subdomains measured by absorbance at 550nm (A550).

Cell

Supplemental Information

**Reversible, Specific, Active Aggregates
of Endogenous Proteins Assemble
upon Heat Stress**

Edward W.J. Wallace, Jamie L. Kear-Scott, Evgeny V. Pilipenko, Michael H. Schwartz,
Pawel R. Laskowski, Alexandra E. Rojek, Christopher D. Katanski, Joshua A. Riback,
Michael F. Dion, Alexander M. Franks, Edoardo M. Airoidi, Tao Pan, Bogdan A. Budnik,
and D. Allan Drummond

Supplemental Information to: Reversible, specific, active aggregates of endogenous proteins assemble upon heat stress, Wallace et al., *Cell*, 2015

S1 Extended Experimental Procedures

S1.1 Comparison to previous proteome-scale measurements of heat-induced protein aggregation

Our rapid kinetic measurements capture aggregation behavior distinct from that observed after longer stresses. As reported in the main text, our conditions capture aggregation in the majority of known heat-shock granule components forming at the same timescale. A recent study reported 117 proteins forming aggregates after two hours at 42°C (O’Connell et al., 2014); in these data, Pab1 is the only HSG component identified. We detect 90 of these 117 proteins, yet identify aggregation in only three (Pab1, Ura8, Tum1). These results indicate that aggregation measured at different times differs, or that the experimental protocols are incompatible. The two-hour measurements occur long after production of molecular chaperones, whose presence is expected to remodel, reverse, and prevent further aggregation of many proteins; by contrast, our measurements precede detectable induction of molecular chaperones.

S1.2 Yeast growth, heat shock, and cell fractionation

Yeast strain BY4741 was grown, with shaking, at 30°C in SC complete media in a baffled Erlenmeyer flask, to mid-exponential phase ($OD_{600} \approx 0.5$). 50 mL cell culture was transferred to a 50 mL conical tube and centrifuged for 1 min at $2,500 \times g$ at RT, and the media decanted. The tube containing cell pellet with residual medium was placed in a water bath at specified temperature (30°C, 37°C, 42°C, 46°C) for the specified amount of time (0, 2, 4, 8 minutes), after which the pellet was resuspended in 1 mL ice-cold Buffer S0 (120 mM KCl, 2 mM EDTA, 20 mM HEPES-KOH, pH 7.4), transferred to a chilled 1.5 mL microcentrifuge tube, and centrifuged again for 30 seconds at $5,000 \times g$, 4°C. The supernatant was discarded and pellet was resuspended in 100 μ L Buffer S [Buffer S0 + 0.5mM DTT, 1:100 protease inhibitor cocktail IV (Calbiochem 539136), 1mM PMSF], divided in half and flash-frozen into two half-aliquots. One aliquot here became the total protein sample (T), resuspended in 400 μ L Buffer T [20mM HEPES-NaOH, pH7.4, 150 mM NaCl, 3% SDS, 5 mM EDTA, 2 mM DTT, 1:100 PMSF, 1:1000 protease inhibitors IV), and lysed by boiling for 20 minutes at 95°C and vortexing. The other aliquot was placed in a 2 mL Eppendorf “Safe-Lok” tube containing a 7 mM stainless steel ball (Retsch) pre-chilled in liquid nitrogen (LN). Cells were lysed with $4 \times 90s \times 30Hz$ pulses in a Retsch MM100 mixer mill, chilling in LN between pulses. 400 μ L ice-cold Buffer S was added, then the thawed lysate was clarified by centrifugation at $3,000 \times g$ for 30 seconds at 4°C. The clarified supernatant was transferred to a 1.5mL ultracentrifuge tube, and centrifuged at $100,000 \times g$ for 20 minutes at 4°C; the aqueous portion of this is the supernatant (S) sample. The pellet was washed in 500 μ L Buffer S, and centrifuged again at $100,000 \times g$ for 20min at 4°C. The remaining pellet was mixed with 500 μ L Buffer P [8 M urea, 20 mM HEPES-NaOH, pH7.4, 150 mM NaCl, 2% SDS, 2 mM EDTA, 2 mM DTT, 1:100 PMSF, 1:1000 protease inhibitors IV), by vortexing vigorously for 30 minutes. The resuspended pellet was centrifuged at $20,000 \times g$ at RT for 5 minutes, and the aqueous phase was designated as the pellet (P) fraction. Protein from total, supernatant, and pellet fractions was precipitated by chloroform/methanol extraction (Wessel and

Flügge, 1984).

SILAC recovery assay

Yeast auxotrophic for arginine and lysine (RK) were grown with light (rep. 2, heavy) isotope labeled RK (Cambridge Isotope Laboratories) at 30°C to mid-exponential phase, transferred to heavy (rep 2, light) isotope labeled RK, heat shocked for 10 minutes at 42°C, and allowed to recover at 30°C for 0, 20, 60 or 180 minutes. For the 180 minute timepoint in rep 2, cells were diluted in pre-warmed labeled media to ensure they stayed in exponential phase. Cells were harvested, mixed evenly with unheated cells grown in medium-isotope-labeled RK, and flash-frozen. Mixed samples were lysed and fractionated as above, and only the supernatant fraction was chloroform-methanol extracted, trypsin digested, and submitted for LC-MS/MS.

S1.3 Sample preparation for mass spectrometric analysis

Samples were measured to 100 μ g of total protein each. Samples were digested with trypsin using a FASP protocol (Wiśniewski et al., 2009). For dimethyl labeling of T, S, P, samples, digested samples were labeled as described by Boersema et al. (2009); total was labeled +28Da (light), supernatant was labeled +32Da (medium), and pellet was labeled +36Da (heavy). Subsequently, T, S, P, samples from the same experiment were mixed evenly.

An aliquot of each sample was taken, and submitted directly for mass spectrometry analysis. The remaining sample was fractionated by high-performance liquid chromatography (HPLC). The HPLC 1200 Agilent system with fraction collector (Agilent Technologies, Santa Clara, CA) was used for ERLIC (electrostatic repulsion-hydrophilic interaction chromatography, Alpert (2008)) separation on a PolyWAX LP column (200 x 2.1 mm, 5 μ m, 300, PolyLC Inc, Columbia, MD). Sample was fractionated into 20 fractions on a 70 minute LC gradient. Individual or combined fractions were submitted for mass spectrometry analysis.

S1.4 Mass spectrometry

Mass spectra were measured on an Orbitrap Velos Pro (Thermo Fisher, San Jose, CA). Samples injected from an autosampler (Waters, NanoAquity, Milford, MA) were loaded into the trapping column (75 μ m column ID, 5 cm packed with 5 μ m beads on 200 pores, from Michrom Bioresources, Inc.), washed for 15 minutes and then eluted to an analytical column with a gradient from 2 to 32% of buffer B [0.1% formic acid in acetonitrile] over a 90 minute gradient for each fraction. Instrument was set up to run TOP 20 method for MS/MS in the ion trap with an exclusion function turned on, followed by a MS1 scan in Orbitrap with 60K resolving power at mass of 400 m/z.

Obtained runs were analyzed jointly by MaxQuant Software, version 1.5.0.30 (Cox et al. (2011), <http://maxquant.org/>). Searches were done against verified and uncharacterized ORFs from the R64-1-1 release of the S288C genome proteome database (yeastgenome.org), and common contaminants added to the database from the Global Proteome Machine (<http://www.thegpm.org/crap/>). Searches were done with trypsin enzyme specificity, allowing 2 missed cleavages. Possible modifications included in the search parameters were: protein N-terminus acetylation, methionine oxidation, deamidation of asparagine and glutamine amino acids, and phosphorylation of serine, threonine, and tyrosine. For triplex dimethyl labeling, labels on primary amines for light (+28 Da), medium (+32 Da) and heavy (+36 Da) were searched for as variable modifications. For SILAC, labels of medium lysine (+4 Da), heavy lysine (+8 Da), medium arginine (+6 Da) and heavy arginine (+10

Da) were searched for as variable modifications. The database search criteria were held at 1% FDR on both protein and on peptide levels for all output reported data. All parameters for MaxQuant runs are supplied in the Dryad package.

We used MaxQuant intensities from the evidence.txt file, not the reported ratios which are calculated using a different method, because we noted a detection-intensity-dependent bias in ratios that was largely absent from the quotient of the intensities.

S1.5 Statistical analysis

MaxQuant reports intensities in three channels per detection event: light (L), medium (M), and heavy (H), which in this experimental design are noisy proxies for total sample (T), 100,000 × g supernatant (S), and 100,000 × g pellet (P) respectively. Our goal is to estimate the proportion in supernatant (pSup), the ratio of supernatant to total, for each protein individually, which is a number between 0 and 1. This is complicated by measurement noise in the data, principally that the separate samples undergo multiple processing steps in parallel before being mixed and measured by mass spectrometry, so that the ratios measured on the machine are not stoichiometric compared to the original ratios in cell lysate. For example, directly estimating the S/T ratio from the M/L ratio produces estimates greater than 1; conversely, we can employ conservation of mass (in cells, for each protein $T = S + P$) to constrain models in order to fit the data accurately.

We employed multiple statistical analyses to estimate pSup, finding that correcting for uneven fraction mixing, batch effects, and other measurement noise produces the most biologically coherent quantitative picture of protein aggregation across multiple biological replicates, while agreeing in outline with more naive analyses. Three alternative estimates of pSup are shown in figure S1. The first, called M/(M+H), simply takes the median across peptides of intensity ratios. The second, called model 2 (m.2), uses conservation of mass and an error model, applied to each experiment independently, to correct for uneven mixing and estimate confidence intervals. The third, called model 3 (m.3), corrects for batch effects in biochemical separation by normalizing the pSup across experiments for a subgroup of proteins. We found that all models agree in outline and produce high correlation (Pearson’s r coefficient) between biological replicates, although model 2 successfully accounts for conservation of mass, and model 3 was better at reducing bias and root-mean-squared-error (RMSE), as shown in figure S1. In particular, model 3 reduced batch-effect variation between measurements of one biological sample with multiple treatments (30C.rep1, 46C.2min, 46C.4min, 46C.8min) and another collected at a different time and measured in less depth (30C.rep3, 37C.8min, 42C.8min). We use the output of model 3 as pSup estimates in all figures in this paper except as noted in fig. S1.

S1.5.1 Technical details of statistical models

The goal of the statistical analysis is to estimate proportion in supernatant (pSup), the ratio of supernatant to total. The measurement noise has three components, all acting multiplicatively. The first noise component captures the fact that the proportions of each sample (T, S, P) as mixed and measured differ from their original proportions in cell lysate, since samples are extracted, digested and labeled separately; we call these the mixing ratios, and denote them by $\vec{\alpha} = (\alpha_T, \alpha_S, \alpha_P)$. The second noise component quantifies how distinct peptide states from a single protein may have highly variable intensities; we call this the detectability of events, and denote by γ_{ij} for event j associated with protein i . The third, residual, noise component, denoted by $\epsilon_{C,ij}$, is considered independent across channels $C = (L, M, H)$, and for each detection event j associated with protein i .

The list of quantities needed for an accurate statistical model is as follows:

- i indexes proteins
- r_i proportion in supernatant (pSup) of protein i
- T_i abundance of protein i
- S_i abundance in supernatant of protein i
- P_i abundance in pellet of protein i
- j indexes peptide detection events
- L_{ij} intensity in light channel detected in event j , protein i
- M_{ij} intensity in medium channel detected in event j , protein i
- H_{ij} intensity in heavy channel detected in event j , protein i
- γ_{ij} detectability for event j
- $\epsilon_{L,ij}$ residual noise in L intensity for event j
- $\epsilon_{M,ij}$ residual noise in M intensity for event j
- $\epsilon_{H,ij}$ residual noise in H intensity for event j
- α_T mixing ratio for total fraction
- α_S mixing ratio for supernatant fraction
- α_P mixing ratio for pellet fraction

where $(\alpha_T, \alpha_S, \alpha_P) \in \text{Simplex}$, $r_i \in [0, 1]$ for each i , and the remaining quantities are non-negative. We posit multiplicative lognormal noise in each channel. The full model is as follows.

$$L_{ij} = \alpha_T T_i \gamma_j \epsilon_{T,ij} \quad (1a)$$

$$M_{ij} = \alpha_S S_i \gamma_j \epsilon_{S,ij} \quad (1b)$$

$$H_{ij} = \alpha_P P_i \gamma_j \epsilon_{P,ij} \quad (1c)$$

$$S_i = r_i T_i \quad (1d)$$

$$P_i = (1 - r_i) T_i \quad (1e)$$

The inferential targets are the proportions in supernatant for each protein, $\{r_i\}$.

In fig. S1, model 1 “M/(M+H)” naively estimates $r_i = \text{median}_j \left(\frac{M_{ij}}{M_{ij} + H_{ij}} \right)$, which does not account for the mixing ratios $\vec{\alpha}$ nor use data from the total protein channel.

To estimate r_i , we need not estimate the absolute protein abundances. Thus we consider a restricted model for ratios $\frac{M}{L}$ and $\frac{H}{L}$ in our analysis, as follows.

$$\frac{M_{ij}}{L_{ij}} = \frac{\alpha_S}{\alpha_T} r_i \epsilon_{M/L,ij} \quad (2a)$$

$$\frac{H_{ij}}{L_{ij}} = \frac{\alpha_P}{\alpha_T} (1 - r_i) \epsilon_{H/L,ij} \quad (2b)$$

The restricted model has the advantage that both the absolute protein abundances, $\{T_i\}$, and the detectability parameters, $\{\gamma_{ij}\}$, cancel out, and need not be estimated. We complete the specifications by positing a single noise term per ratio, $\epsilon_{M/L,ij}$ and $\epsilon_{H/L,ij}$, for each event j associated with protein i . This strategy for estimating the proportions in supernatant is akin to a partial likelihood approach.

To complete the model specifications, we posit the following prior distributions:

$$r_i \stackrel{iid}{\sim} \text{Beta}\left(\frac{1}{2}, \frac{1}{2}\right) \quad (2c)$$

$$(\alpha_T, \alpha_S, \alpha_P) \sim \text{Dirichlet}(100, 100, 100) \quad (2d)$$

$$\begin{pmatrix} \ln \epsilon_{M:L,ij} \\ \ln \epsilon_{H:L,ij} \end{pmatrix} \stackrel{iid}{\sim} N\left(0, \begin{pmatrix} \eta_{M:L}^2 & \rho \eta_{M:L} \eta_{H:L} \\ \rho \eta_{M:L} \eta_{H:L} & \eta_{H:L}^2 \end{pmatrix}\right) \quad (2e)$$

$$\eta_{\bullet:L} \sim \text{Cauchy}(0, 1)^+ \quad (2f)$$

$$\rho \sim \text{Beta}(1, 1). \quad (2g)$$

Here we chose a $\text{Beta}(\frac{1}{2}, \frac{1}{2})$ prior for r_i , the Jeffreys prior for the binomial likelihood; after testing a variety of priors we found this to be weakly informative and numerically stable. The Dirichlet prior for $\vec{\alpha}$ is a strong prior that enforces even mixing proportions; since we have thousands of observations the posterior is nevertheless dominated by the data. We chose a half-Cauchy prior distribution for the variance parameters η as this is a sensible default choice for top-level variance parameters (Polson and Scott, 2012). ρ represents the correlation of the M:L and H:L ratios (equations 2a, 2b) due to shared noise from the L channel; if all noise variances are the same in each channel then $\rho = 0$.

We used equations (2a-2g) to estimate values of $\{r_i\}$ jointly with other specified parameters by Markov Chain Monte Carlo (Robert and Casella, 2005). We implemented the sampler using the probabilistic programming language STAN, accessed using the rstan package (Stan Development Team, 2014) in the R software environment (R Core Team, 2014). This output r_i is displayed as pSup, model 2 in fig. S1. All code is provided in the datadryad package.

We fit model 2 to each experiment individually. Subsequently, we found discrepancies in certain datasets consistent with compression of dynamic range (fig. S1), presumably due to less efficient separation, an artifact of the mass spectrometric measurement and MaxQuant analysis, or other batch effects. To correct for this, we chose lists of proteins reliably in the supernatant (≥ 2 peptides detected in every experiment, and $r_i > 0.9$ in 30C.rep1 and 46C.8min) or reliably in the pellet (≥ 2 peptides detected in every experiment, and $r_i < 0.1$ in 30C.rep1 and 46C.8min), with median r_i 's F_S and F_P respectively across the 30C.rep1 and 46C.8min datasets. Then, we normalized so that these proteins had the same pSup across all experiments, with a linear transformation in log-odds space. Precisely, for a given experiment, f_S is the median r_i for reliably supernatant proteins and f_P for reliably pelleted proteins, and

$$g(r) = \log\left(\frac{r}{1-r}\right) \quad (3)$$

is the logistic function, we transformed:

$$r'_i = g^{-1}\left(g(F_P) + [g(r_i) - g(f_P)] \frac{g(F_S) - g(F_P)}{g(f_S) - g(f_P)}\right). \quad (4)$$

This output r'_i is displayed as pSup, model 3 in fig. S1 and reported in the data package, along with 95% confidence intervals. As the figure shows, it is a minor adjustment in most datasets, and generally reduces the inter-dataset bias and RMSE without obscuring the signal of heat-dependent aggregation. 95% confidence intervals from model 2 were transformed by applying the same equation and parameters to the endpoints. Processing code/scripts and intermediate data are included in the data package.

S1.6 Statistical analysis for SILAC recovery data

In the SILAC recovery assay, we again used MaxQuant Software, version 1.5.0.30 (Cox et al., 2011). We searched for SILAC-labeled arginine and lysine as standard, otherwise using the same variable protein modifications as above. We report median ratios of MaxQuant-estimated intensities, correcting for deviations from even mixing by fixing the median ratio to 1 for proteins reliably found in the supernatant in the aggregation assay previously. This code is also available in the data package.

S1.7 Sedimentation coefficients of pelleting particles

Here we estimate the particle sizes expected to sediment in our assay. Centrifugation conditions are acceleration $a = 100,000g \approx 10^6 ms^{-2}$ for $t = 20mins \approx 10^3s$.

0.5mL of liquid in a 1.5mL eppendorf tube is approximately $d = 2cm = 2 \times 10^{-3}m$ high, so particles pellet if:

$$v = d/t \geq \frac{2 \times 10^{-3}m}{10^3s} = 2 \times 10^{-6}ms^{-1} \quad (5)$$

since the sedimentation coefficient $c = v_t/a$, that implies that

$$c \geq \frac{2 \times 10^{-6}ms^{-1}}{10^6ms^{-2}} = 2 \times 10^{-11}s = 200S \quad (6)$$

as a Svedberg unit $S = 10^{-13}s$.

This rough estimate suggests that the smallest pelleting particles should be much larger than 80S ribosomes, consistent with our observations.

S1.8 Protein annotation

Annotation of protein groups used in figures 1 and S4, were derived from the Saccharomyces Genome Database (Cherry et al., 2012) for most groups, from the sources listed in table S2 for heat shock granule components, and from computational structure prediction for Membrane proteins.

Glycolytic enzymes are: Hxk1, Hxk2, Pgi1, Pfk1, Pfk2, Fba1, Tpi1, Tdh3, Tdh2, Tdh1, Pgi1, Gpm1, Eno1, Eno2, Cdc19, Pyk2.

Ribosomal proteins annotated here include only core components, whose names in yeast begin Rpl for the large subunit, Rps for the small subunit, and Rpp for the stalk.

Our list of nucleolar proteins is manually curated from the gene ontology category (Cherry et al., 2012), as proteins whose *principal* function is nucleolar. There are 143 well-detected nucleolar proteins: Mak16, Utp20, Mak5, Enp1, Spb1, Krr1, Bud23, Pwp2, Rsa4, Csm1, Ycr087c-a, Nop1, Dbp10, Tsr1, Nop14, Sas10, Nhp2, Nop6, Fal1, Mak21, Rrp8, Arx1, Fob1, Rpa14, Hmo1, Bfr2, Ssf2, Utp4, Fcf1, Esf1, Utp5, Utp6, Snu13, Pol5, Nop16, Nug1, Utp7, Spb4, Loc1, Cdc14, Dbp3, Prp43, Rok1, Utp22, Nop7, Utp8, Enp2, Mtr3, Nsr1, Nop19, Efg1, Pxr1, Ygr283c, Rrp3, Ssf1, Nop10, Rpf1, Gar1, Rpc10, Imp3, Dbp8, Utp9, Air1, Utp25, Rrt14, Nop9, Hca4, Mtr4, Utp18, Net1, Utp10, Rpa34, Mpp10, Urb2, Rpa12, Mrt4, Urb1, Dhr2, Rrp14, Utp11, Rrn3, Ebp2, Tof2, Dbp7, Las1, Rpf2, Srp40, Drs1, Sof1, Rix7, Noc3, Rlp24, Fcf2, Dip2, Acs2, Cbf5, Emg1, Pwp1, Nop56, Rsa3, Utp13, Ifh1, Dbp9, Utp21, Fpr4, Fpr3, Utp14, Utp15, Ecm16, Rrb1, Rrp5, Tma23, Has1, Rlp7, Imp4, Nop15, Rpc19, Kre33, Nop13, Ubp10, Rpa49, Trf5, Kri1, Dbp6, Nog2, Esf2, Rcl1, Nop12, Brx1, Pap2, Nop8, Utp23, Bud21, Pno1, Ytm1, Rrs1, Nop58, Rpa43, Rpa190, Nop4, Nog1, Nan1, Nop53, Nip7, Bms1, Dim1, Rpa135, Tif6, Mrd1, Rrp9, Rrp15, Noc4.

Our list of membrane proteins includes those with at least 2 transmembrane domains identified by TMHMM 2.0 (Krogh et al., 2001). There are 268 well-detected membrane proteins: Aus1, Ccc1, Drs2, Rcf2, Erg11, Sna2, Yro2, Gup1, Ftr1, Eos1, Gaa1, Rsn1, Tda5, Csg2, Sft2, Tvp38, Chs2, Alg9, Adp1, Nce102, Gpi11, Erp2, Sal1, Spf1, Dip5, Nsg1, Pmt7, Ecm3, Dfm1, Ssh1, Pmt3, Dnf1, Cst26, Sly41, Izh2, Erg3, Ale1, Pam17, Yip3, Gpi14, Tul1, Mal11, Neo1, Mdl1, Alg12, Dpp1, Ste24, Pdr15, Vma3, Erp5, Fat1, Tcb1, Hip1, Rtn1, Tsc13, Avt3, Ymd8, Aim26, Ost2, Ste2, Qdr2, Fre1, Vtc2, Vcx1, Lnp1, Shy1, Atg33, Kha1, Lac1, Sec61, Fth1, Dfg10, Atm1, Nnf2, Zrt2, Yor1, Zrt1, Flc1, Sam3, Cds1, Nte1, Pmc1, Ncr1, Gpt2, Pma1, Vtc3, Lem3, Ndc1, Cpt1, Fks1, Brl1, Hmg2, Lyp1, Atr1, Mup1, Cox15, Usa1, Tat1, Ena1, Sec62, Ypk9, Sey1, Tna1, Ost5, Aur1, Itr1, Ost3, Ssm4, Gdt1, Bap2, Zrc1, Ptr2, Sac1, Pmr1, Pom152, Hmg1, Pdr5, Fre7, Alr2, Pmt1, Enb1, Agp1, Emc4, Cho2, Sur2, Fks3, Emp24, Chs1, Ybt1, Gpi17, Yos1, Erv29, Ecm33, Hxt5, Dnf3, Gex2, Chs3, Tvp18, Svp26, Vma9, Cwh43, Pma2, Cos10, Alg2, Scs7, Gtt3, Rer1, Aac1, Cdc50, Stt3, Bi4, Ctr1, Spo75, Die2, Alg3, Pom33, Pmt5, Arn2, Pmt6, Tpo1, Hxt1, Cox1, Cox10, Erg4, Vph2, Rcf1, Pdr12, Vtc4, Bpt1, Sur4, Get2, Uip3, Mal31, Cpr8, Pho87, Rax1, Sec63, Hxt16, Mrl1, Swp1, Vmr1, Sdh3, Erg28, Pis1, Fmp37, Nsg2, Erg1, Avt7, Fsf1, Lag1, Set1, Fun26, Ato3, Avt1, Bap3, Mrh1, Yip4, Gpi1, Erv41, Thi72, Lcb3, Pho91, Erp1, Cox2, Crd1, Trk1, Akr1, Ptm1, Mnr2, Hxt6, Gsc2, Pmt2, Emc1, Ist2, Ycf1, Pet9, Vph1, Yip5, Yif1, Smf3, Emp70, Fen1, Fcy21, Ost6, Flc2, Yet1, Tpo4, Aim14, Pga3, Erj5, Ypq1, Ole1, Erd2, Rbd2, Aac3, Stv1, Pex31, Yct1, Sur7, Vba4, Mcd4, Dnf2, Gup2, Tpo3, Gab1, Pmt4, Syg1, Ste6, Hxt10, Tmn3, Mtc7, Gnp1, Spc1, Yop1, Rim21, Snq2, Cdc1, Cho1, Yet3, Elo1, Erv14, Mdl2, Hxt3, Flc3, Pho86, Msc2, Spc2, Dal4.

Our list of molecular chaperones is: Ssa1, Ssa2, Ssa3, Ssa4, Ssb1, Ssb2, Sse1, Ssz1, Hsp26, Hsp42, Hsp82, Hsc82, Hsp104, Zuo1, Sse2, Fes1, Ydj1, Sis1, Hsp78, Ssc1, Kar2, Sil1, Hch1, Aha1, Sba1, Stil.

S1.9 Strains

To construct fluorescently tagged strains for microscopy, plasmids pJLS033 and pJLS035 were constructed for C-terminal Clover and mRuby2 labeling at the native locus. Clover/mRuby2.KanMX cassette PCR fragments were transformed into BY4741 and BY4742 according to standard lithium acetate protocol and selected using G418. Diploids were generated by crossing PCR-confirmed positives for 4 hours at RT, then overnight at 30°C on YPD, followed by selection on SC –cys –met –lys plates. All strains used are listed in Table S6.

S1.10 Spinning-disk confocal fluorescence microscopy

Cells were grown to mid-log phase ($\approx 3 \times 10^7$ cells/mL) in non-fluorescent synthetic yeast growth medium (NSD; per 1 L: 20 g glucose, 5 g ammonium sulfate, 0.79 g CSM [Sunrise Science Products #1001-100], 1.7 g YNB trace elements [US Biological Y2035-01], 2 mL 500x non-fluorescent vitamin mix [500 mg calcium pantothenate, 2.5 g myo-inositol, 100 mg niacin, 50 mg p-aminobenzoic acid, 100 mg pyridoxine hydrochloride, 100 mg thiamine hydrochloride, dH₂O to 500 mL, filter sterilized], 2 mL 500x biotin (0.2 g/L), 2 mL 500x CoCl₂-6H₂O (0.1 g/L), 20 mg adenine sulfate). 25 μ L aliquots were heat-treated for 8 minutes at 30°C or 46°C in an Eppendorf Thermomixer. To reduce live cell motion while imaging, coverslips coated with concanavalin-A were applied to base-washed slides to prepare flow-chambers using melted Parafilm (Joglekar et al., 2008). Heat-treated cells were applied to the flow-chamber and allowed to settle before rinsing unbound cells with NSD mounting media and sealing with VALAP (equal parts Vaseline, lanolin, and paraffin wax mixed to homogeneity by gentle heating and applied using a cotton-tipped applicator) to decrease evaporation

of mounting medium.

Images were captured with a 100 \times /1.45 oil objective on Olympus DSU spinning disk confocal microscope (Olympus Corporation of the Americas, Center Valley, PA) with a Hamamatsu model C9100 EM-CCD camera (Hamamatsu Photonics, Skokie, IL) controlled by SlideBook v5.0 software (Intelligent Imaging Innovations, Denver, CO). Filter sets were FITC/Cy2 (excitation 490/20 nm, emission 528/38 nm) for Clover and DsRed (excitation 565/25 nm, emission 624/40 nm) for mRuby2. 20 plane z -stacks were collected over a range of 4.94 μm (step size 0.26 μm). Fluorescence images were deconvolved in Fiji software (Schindelin et al., 2012) using the deconvolution lab plugin (Vonesch and Unser, 2008) to perform 10 iterations of the Richardson-Lucy algorithm, subtracting minimal intensity background and using point-spread functions generated for the Olympus DSU microscope by PSF generator software (Kirshner et al., 2013). Then, using Fiji, a single slice from the deconvolved stack was selected, a 20 μm \times 20 μm square selected, and intensity automatically adjusted (ImageJ macro provided upon request); the corresponding single-slice square from the DIC images was selected alongside.

S1.11 Protein gel electrophoresis

Samples were first boiled in Laemmli buffer (BioRad #161-0737), and aliquots (5 μL unless otherwise noted) were loaded onto 4-15 % Criterion TGX (BioRad #567-1084). Gels were run at 200V for 40 minutes in a Bio-Rad Criterion system. Coomassie staining was performed using Gelcode Blue (Thermo #24592) according to manufacturer's instructions. Gels were imaged using a Chemidoc-MP (Bio-Rad).

S1.12 Western blotting

Proteins were transferred to 0.2 μm nitrocellulose membranes (BioRad #9004-70-0) in Towbin buffer using the Criterion blotter system (Bio-Rad). Protein was detected using 2.5 μg anti-Pab1 antibody (EnCor; Gainesville, FL; #MCA-1G1), or 5 μg anti-Ssz1 antibody (Hundley et al., 2002), along with the ONE-HOUR WesternTM Basic Kit (Mouse; GenScript #L00205) according to manufacturer's instructions, and imaged on a Chemidoc-MP (Bio-Rad).

S1.13 Purification of multisynthetase complex components

Unless otherwise stated, cells of *E. coli* strain BL21 (DE3) were grown in LB at 37°C.

Arc1

The full-length Arc1 gene from *S. cerevisiae* was cloned into the pET28a vector using standard cloning methodology, and subsequently transformed into BL21 cells for expression as a fusion with an N-terminal 6-His tag. A single colony was used to inoculate 50 mL LB supplemented with kanamycin (50 $\mu\text{g}/\text{mL}$), and culture was grown to mid-log phase at 37°C prior to 2% inoculation of 1 L fresh LB + kanamycin. IPTG was added to a final concentration of 1 mM when the culture reached $OD_{600} = 0.75$, at which time the flask was transferred to 30°C incubator with shaking at 200 RPM for 4 hours. Cells were pelleted at 5000 $\times g$ for 10 minutes at 4°C, then resuspended in 20 mM HEPES (pH 7.4), 120 mM KCl, 5 mM imidazole, 0.2% Triton X-100, 0.5 mM β -mercaptoethanol, and EDTA-free complete protease inhibitor tablets (Roche 05 056 489 001), then lysed on ice/water bath with sonication 7 seconds ON/7 seconds OFF cycles for 20 minutes at 60% amplitude. Cell debris and insoluble material was removed via centrifugation for 20 minutes at 18,000 $\times g$, 4°C.

Clarified lysate was loaded onto a buffer-equilibrated 5 mL HiTrap Chelating HP column (GE Healthcare Life Sciences 17-0409) on an ÄKTAprime system (GE Healthcare Life Sciences) with automated fraction collector. The column was washed with 5 column volumes (CV) of buffer containing 20 mM HEPES, 120 mM KCl, 30 mM imidazole, then bound proteins were eluted over a 40 mL gradient (0-100%) to buffer containing 20 mM HEPES, 120 mM KCl, 300 mM imidazole. Fractions containing Arc1 were pooled and buffer exchanged to 50 mM Na₂HPO₄, pH 6.7, prior to loading onto a 5 mL HiTrap SP HP column (GE Healthcare Life Sciences 17-1151-01). The column was washed with 5 CV of buffer containing 50 mM Na₂HPO₄, pH 6.7, and Arc1 was eluted over a 35 mL gradient (0-100%) to buffer containing 50 mM Na₂HPO₄, 1M NaCl, pH 6.7. Fractions containing Arc1 were pooled, buffer exchanged to buffer A [20 mM HEPES, 150 mM KCl, , pH 7.4], concentrated and further purified on Superose 6 10/300 GL column (GE Healthcare Life Sciences) equilibrated with buffer A using ÄKTApurifier FPLC system (FPLC; GE Life Sciences). Arc1 was eluted at 15.8 ml and 0.5 ml peak fraction was divided into aliquots, frozen, and stored at -80°C until used.

Mes1

The protocol is the same as for Arc1, with the following exceptions. Culture was grown in TB medium [1.2% peptone, 2.4% yeast extract, 0.4% glycerol, 72 mM K₂HPO₄, 17 mM KH₂PO₄] and induced at $OD_{600} = 0.4$ with 1 mM IPTG at 20°C for 5 hours. Cells were lysed in buffer containing 20 mM HEPES, 250 mM KCl, 20 mM imidazole, 0.5 mM β -mercaptoethanol, 0.5% Chaps detergent and EDTA-free complete protease inhibitor tablets, pH 7.4]. HiTrap Chelating HP column was washed with buffer containing 20 mM HEPES, 250 mM KCl, 20 mM imidazole, pH 7.4 and bound protein was eluted using buffer containing 20 mM HEPES, 250 mM KCl, and 400 mM imidazole, pH 7.4]. Fractions containing Mes1 were pooled, buffer exchanged to 20 mM HEPES (pH 7.4), 80 mM KCl, applied to monoQ 5/50 GL column and fractions were collected across a 10 ml 80-600 mM KCl gradient by FPLC. Mes1 containing fraction (eluted between 300 and 400 mM KCl) was then applied to Superdex 200 10/300 GL equilibrated with buffer A and 0.5 ml fractions were collected following elution by FPLC. Mes1 was eluted at 14.0 ml and peak fractions were concentrated, divided into aliquots, frozen, and stored at -80°C until used.

Gus1

The protocol is the same as for Arc1, with the following exceptions. Cells were induced at $OD_{600} = 0.75$ with 1 mM IPTG at 20°C for 5 hours. Cells were lysed in buffer containing 20 mM HEPES, 140 mM KCl, 20 mM imidazole, 0.5 mM β -mercaptoethanol, 0.2% Triton X-100 and EDTA-free complete protease inhibitor tablets, pH 7.4]. HiTrap Chelating HP column was washed with buffer containing 20 mM HEPES, 140 mM KCl, and 20 mM imidazole, pH 7.4 and bound protein was eluted using buffer containing 20 mM HEPES, 140 mM KCl, and 400 mM imidazole, pH 7.4]. Fractions containing Gus1 were pooled and buffer exchanged to 20 mM bis-tris propane, pH 7.1, then loaded onto a 5 mL HiTrap Q HP column (GE Healthcare Life Sciences 17-1154-01). Column was washed with buffer containing 20 mM bis-tris propane, pH 7.1, and eluted using 20 mM bis-tris propane, 1 M NaCl, pH 7.1. Fractions containing Gus1 were pooled, buffer exchanged to buffer A, concentrated and further purified on Superose 6 10/300 GL column using FPLC. Gus1 was eluted at 16.2 ml and 0.5 mL peak fraction was divided into aliquots, frozen, and stored at -80°C until used.

Isolation and heat-assembly of AME multisynthetase complex

Purified Mes1, Arc1, Gus1 were mixed in a 1:1:1 molar ratio in a total volume of 0.5 mL in a buffer containing 20 mM HEPES (pH 7.4), 150 mM KCl, 5 mM MgCl₂, incubated for 12 hours at 4°C, then spun down at 10,000 × *g* for 10 minutes at 4°C prior to loading on a Superdex200 column equilibrated with buffer B (20 mM HEPES [pH 7.0], 150 mM KCl, 0.1 mM MgCl₂). AME complex was collected upon elution from the column at 11.3 mL and subsequently concentrated and stored at 4°C.

All reactions were assembled to contain 4 μM AME (or 2μM Mes1) in buffer 20 mM HEPES (pH=7.0), 150 mM KCl, 2 mM MgCl₂ and incubated 15 min at either 30°C or 46°C followed by dilution (when indicated) and further 1 hr incubation at indicated temperature. Reactions were centrifuged at 100,000 *g* for 20 min and supernatant transferred to a clean tube. The pellets were washed once with 200 μL of 20 mM HEPES (pH=7.0), 150 mM KCl, 2 mM MgCl₂ and centrifuged again. Pellets were resolubilized in Laemmli buffer and proportional amounts of T and S material diluted with 2× Laemmli were subjected to PAGE and staining. Heated samples were diluted 40× with 20 mM HEPES (pH=7.0), 150 mM KCl, 2 mM MgCl₂ followed by 1 hr incubation at 30°C, and in a separate sample additionally supplemented with (cold) methionine and yeast total tRNA as in aminoacylation reactions followed by 1 hr incubation at 30°C.

Dynamic light scattering

Dynamic light scattering (DLS) measurements were performed using a DynaPro Nanostar (Wyatt Technology). Protein samples at 5–6 μM in aggregation buffer were incubated at 20°C and centrifuged at 21,000 *g* for 30min prior to the measurements, equilibrated and verified for stability in DLS at 25°C, and then the temperature was ramped to 50°C at 0.25°C per minute. Each timepoint was measured five times, with an acquisition time of 6s, filtered for only those runs with a baseline deviation of less than 0.003 to remove spurious readings. The apparent hydration radii reported are cumulant radii calculated using Dynamics software (Wyatt Technology).

Absorbance

For aggregation studies, absorbance data was collected on a Jasco J-715 spectropolarimeter equipped with Jasco PFD-425S temperature control unit. Proteins were dialyzed into assay buffer (20mM HEPES, 175mM KCl, pH 7.4) and this buffer alone was preheated to the desired temperature in a 1cm quartz cuvette, with a magnetic stir bar at full speed to prevent settling of large particles during the experiment. Protein sample at the desired concentration was added after temperature equilibration, and 550nm absorbance readings were collected at 1-second intervals. Absorbance differences were calculated by subtracting the minimum of the first five readings.

Supernatant/pellet fractionation of AME

Aminoacylation assay

Filter-based aminoacylation reactions were performed at 30°C in 20mM HEPES-KOH, 150mM NH₄Cl, 100uM cold Met, 10mM MgCl₂, 0.1mM EDTA, 5mM DTT, 4mM ATP, 0.5 μCi/μL ³⁵S-methionine, 40 μM total yeast tRNA and AME or Mes1 enzyme. Heat shock was performed on enzymes at 4μM at 46°C for 15 minutes or 95°C for 5 minutes immediately prior to the aminoacylation reaction, then diluted to 10× the reaction concentration. Reactions were run for 10 minutes

and quenched in cold 10 % trichloroacetic acid (TCA) before spotting on filter disks in a vacuum apparatus. Filters were washed with 2 mL cold 10 % TCA and 1 mL cold ethanol, dried, and exposed to a phosphorimager screen for quantification with ImageLab software (BioRad).

Aminoacylation reactions for tRNA microarray analysis were performed at 30°C in 50 mM HEPES KOH (pH 7.5), 100 mM potassium glutamate, 10 mM magnesium acetate, 1 mM DTT, 2 mM ATP, 2.5 $\mu\text{Ci}/\mu\text{L}$ ^{35}S -methionine, 40 μM total yeast tRNA and 1 μM AME enzyme prepared as above. Microarray analysis of tRNA charging was performed as previously described (Netzer et al., 2009; Wiltout et al., 2012).

Supplementary References

- Alexa, A., Rahnenführer, J. and Lengauer, T. (2006). Improved scoring of functional groups from gene expression data by decorrelating GO graph structure. *Bioinformatics* 22, 1600–7.
- Alpert, A. J. (2008). Electrostatic repulsion hydrophilic interaction chromatography for isocratic separation of charged solutes and selective isolation of phosphopeptides. *Anal Chem* 80, 62–76.
- Boersema, P. J., Raijmakers, R., Lemeer, S., Mohammed, S. and Heck, A. J. R. (2009). Multiplex peptide stable isotope dimethyl labeling for quantitative proteomics. *Nat Protoc* 4, 484–94.
- Brachmann, C. B., Davies, A., Cost, G. J., Caputo, E., Li, J., Hieter, P. and Boeke, J. D. (1998). Designer deletion strains derived from *Saccharomyces cerevisiae* S288C: a useful set of strains and plasmids for PCR-mediated gene disruption and other applications. *Yeast* 14, 115–32.
- Cherkasov, V., Hofmann, S., Druffel-Augustin, S., Mogk, A., Tyedmers, J., Stoecklin, G. and Bukau, B. (2013). Coordination of translational control and protein homeostasis during severe heat stress. *Curr Biol* 23, 2452–62.
- Cherry, J. M., Hong, E. L., Amundsen, C., Balakrishnan, R., Binkley, G., Chan, E. T., Christie, K. R., Costanzo, M. C., Dwight, S. S., Engel, S. R. et al. (2012). *Saccharomyces* Genome Database: the genomics resource of budding yeast. *Nucleic Acids Res* 40, D700–5.
- Cox, J., Neuhauser, N., Michalski, A., Scheltema, R. A., Olsen, J. V. and Mann, M. (2011). Andromeda: a peptide search engine integrated into the MaxQuant environment. *J Proteome Res* 10, 1794–805.
- Gerashchenko, M. V. and Gladyshev, V. N. (2014). Translation inhibitors cause abnormalities in ribosome profiling experiments. *Nucleic acids research* 42, e134.
- Grousl, T., Ivanov, P., Frýdlová, I., Vasicová, P., Janda, F., Vojtová, J., Malínská, K., Malcová, I., Nováková, L., Janosková, D. et al. (2009). Robust heat shock induces eIF2 α -phosphorylation-independent assembly of stress granules containing eIF3 and 40S ribosomal subunits in budding yeast, *Saccharomyces cerevisiae*. *J Cell Sci* 122, 2078–88.
- Grousl, T., Ivanov, P., Malcova, I., Pompach, P., Frydlova, I., Slaba, R., Senohrabkova, L., Novakova, L. and Hasek, J. (2013). Heat shock-induced accumulation of translation elongation and termination factors precedes assembly of stress granules in *S. cerevisiae*. *PLoS ONE* 8, e57083.
- Holmes, K. J., Klass, D. M., Guiney, E. L. and Cyert, M. S. (2013). Whi3, an *S. cerevisiae* RNA-binding protein, is a component of stress granules that regulates levels of its target mRNAs. *PLoS ONE* 8, e84060.

- Hundley, H., Eisenman, H., Walter, W., Evans, T., Hotokezaka, Y., Wiedmann, M. and Craig, E. (2002). The in vivo function of the ribosome-associated Hsp70, Ssz1, does not require its putative peptide-binding domain. *P Natl Acad Sci Usa* *99*, 4203–8.
- Joglekar, A. P., Salmon, E. D. and Bloom, K. S. (2008). Counting kinetochore protein numbers in budding yeast using genetically encoded fluorescent proteins. *Methods Cell Biol* *85*, 127–51.
- Kirshner, H., Aguet, F., Sage, D. and Unser, M. (2013). 3-D PSF fitting for fluorescence microscopy: implementation and localization application. *Journal of microscopy* *249*, 13–25.
- Krogh, A., Larsson, B., von Heijne, G. and Sonnhammer, E. L. (2001). Predicting transmembrane protein topology with a hidden Markov model: application to complete genomes. *J Mol Biol* *305*, 567–80.
- Netzer, N., Goodenbour, J. M., David, A., Dittmar, K. A., Jones, R. B., Schneider, J. R., Boone, D., Eves, E. M., Rosner, M. R., Gibbs, J. S. et al. (2009). Innate immune and chemically triggered oxidative stress modifies translational fidelity. *Nature* *462*, 522–6.
- O’Connell, J. D., Tsechansky, M., Royall, A., Boutz, D. R., Ellington, A. D. and Marcotte, E. M. (2014). A proteomic survey of widespread protein aggregation in yeast. *Mol Biosyst* *10*, 851–861.
- Polson, N. G. and Scott, J. G. (2012). On the half-Cauchy prior for a global scale parameter. *Bayesian Anal.* *7*, 887–902.
- Pu, S., Wong, J., Turner, B., Cho, E. and Wodak, S. J. (2009). Up-to-date catalogues of yeast protein complexes. *Nucleic acids research* *37*, 825–31.
- R Core Team (2014). *R: A Language and Environment for Statistical Computing*. R Foundation for Statistical Computing Vienna, Austria.
- Rinnerthaler, M., Lejskova, R., Grousl, T., Stradalova, V., Heeren, G., Richter, K., Breitenbach-Koller, L., Malinsky, J., Hasek, J. and Breitenbach, M. (2013). Mmi1, the yeast homologue of mammalian TCTP, associates with stress granules in heat-shocked cells and modulates proteasome activity. *PLoS ONE* *8*, e77791.
- Robert, C. and Casella, G. (2005). *Monte Carlo Statistical Methods*. Springer Texts in Statistics, corrected second edition, Springer-Verlag, New York, NY.
- Schindelin, J., Arganda-Carreras, I., Frise, E., Kaynig, V., Longair, M., Pietzsch, T., Preibisch, S., Rueden, C., Saalfeld, S., Schmid, B. et al. (2012). Fiji: an open-source platform for biological-image analysis. *Nature methods* *9*, 676–682.
- Stan Development Team (2014). *RStan: the R interface to Stan, Version 2.5.0*.
- Swamy, K. B. S., Lin, C.-H., Yen, M.-R., Wang, C.-Y. and Wang, D. (2014). Examining the condition-specific antisense transcription in *S. cerevisiae* and *S. paradoxus*. *BMC genomics* *15*, 521.
- Vonesch, C. and Unser, M. (2008). A fast thresholded Landweber algorithm for wavelet-regularized multidimensional deconvolution. *Image Processing, IEEE Transactions on* *17*, 539–549.
- Wessel, D. and Flügge, U. I. (1984). A method for the quantitative recovery of protein in dilute solution in the presence of detergents and lipids. *Anal Biochem* *138*, 141–3.

- Wiltrout, E., Goodenbour, J. M., Fréchin, M. and Pan, T. (2012). Misacylation of tRNA with methionine in *Saccharomyces cerevisiae*. *Nucleic acids research* *40*, 10494–506.
- Wiśniewski, J. R., Zougman, A., Nagaraj, N. and Mann, M. (2009). Universal sample preparation method for proteome analysis. *Nat Methods* *6*, 359–62.
- Yamamoto, Y. and Izawa, S. (2013). Adaptive response in stress granule formation and bulk translational repression upon a combined stress of mild heat shock and mild ethanol stress in yeast. *Genes Cells* *18*, 974–84.